

Quantum theory of nondegenerate multiwave mixing. III. Application to single-beam squeezed-state generation

Seng-Tiong Ho

AT&T Bell Laboratories, 600 Mountain Avenue, Murray Hill, New Jersey 07974

Prem Kumar

Department of Electrical Engineering and Computer Science, Robert R. McCormick School of Engineering and Applied Science, Technological Institute, Northwestern University, Evanston, Illinois 60208

Jeffrey H. Shapiro

Department of Electrical Engineering and Computer Science, Massachusetts Institute of Technology, Cambridge, Massachusetts 02139

Received January 18, 1990; accepted April 18, 1990

We apply our quantum theory of nondegenerate multiwave mixing [Phys. Rev. A **37**, 2017 (1988)] to squeezed-state generation experiments with two-level atoms. Our main interest is to predict the amount of squeezing achievable with a Doppler-broadened two-level medium. We are particularly interested in the single-beam configuration, in which all four interacting beams are spatially degenerate. We analytically solve the coupled-mode quantum Langevin equations for nondegenerate four-wave mixing. The solutions are used to compute the amount of squeezing. In the computation the effects of pump-probe phase mismatch, collisions, Doppler broadening, and Gaussian-intensity variation are comprehensively taken into account for the first time to our knowledge. Simple rules of thumb as to where one can see squeezing in both degenerate- and nondegenerate-frequency cases are derived by examining the limit of a short medium. We then present the case of an infinitely long medium, in which maximum squeezing is achieved when there is no pump-probe phase mismatch. With the inclusion of pump-probe phase mismatch, however, the maximum amount of squeezing is obtained with a finite-length medium instead. This prompts us to investigate in detail the finite-length medium case. Our results show that the effects of Doppler broadening and Gaussian-intensity variation can be largely circumvented by detuning the pump frequency more than three Doppler half-widths from resonance and that good broadband squeezing can be achieved even with a Doppler-broadened medium that has a moderate amount of collision broadening. Under these circumstances it is found that the effect of pump self-focusing or defocusing will be the major factor that limits the amount of achievable squeezing. In particular, the spatially varying nonlinear refractive indices seen by the pump and the probe modes are quite different, which causes the former to become spatially mismatched with the latter in the region in which strong squeezing is otherwise expected.

1. INTRODUCTION

In the first paper¹ of this series on the quantum theory of nondegenerate multiwave mixing, we solved for the c -number atomic polarization variable $V_i(t)$ of the i th atom in a system of stationary two-level atoms. We did so in the limit wherein superradiance could be neglected; the effects of spontaneous emission and soft atomic collisions were included in the model. The solution for $V_i(t)$, in terms of the multimode-field Fourier amplitudes $\{A_k(\bar{r}_i)\}$, was derived without the need for an adiabatic approximation.

In the second paper of this series² we used the slowly varying amplitude approximation to express the polarization $V_i(t)$ in terms of the c -number field annihilation and creation variables $\{\alpha_m(t), \alpha_m^+(t)\}$. This procedure is similar to the usual techniques of adiabatic approximation but is more exact in the sense that the effects of dispersion can be taken into account. The slowly varying amplitude approximation allowed us to obtain a set of Langevin equations for the field creation and annihilation variables.

The correlations of the c -number Langevin forces were derived for the special case of nondegenerate four-wave mixing under conditions that permitted nonnegligible atomic collisions. In order to apply the formalism to a traveling-wave geometry, we developed a slowly varying envelope method to deal with quantum field propagation.

The main theme of this paper is the application of the results of Ref. 2 to squeezed-state generation experiments that use four-wave mixing, specifically to the case in which all four waves are spatially degenerate. Physically, in such a case, a single pump beam propagates through a Doppler-broadened two-level medium; vacuum fluctuations are the inputs for the two temporally nondegenerate probe waves. Our interest in the single-beam scheme arises from its simplicity: One does not need to worry about the alignment of the four different beams. This simplicity allows us to compare the experimental results³ with theory with much less uncertainty. In this application the effects of atomic collisions, pump-probe phase

mismatch, Doppler broadening, and Gaussian-beam pump-intensity variation are comprehensively taken into account for the first time to our knowledge. The effect of pump-beam self-focusing and defocusing is also examined.

We begin in Section 2 of this paper by recapitulating the pertinent results of Ref. 2. This is done to make this paper self-contained and to reestablish the notation. The remainder of this paper can be divided into four parts. In the first part, Sections 3 and 4, we assume time stationarity and solve the spatial coupled-mode equations for the c -number mode-amplitude variables $\{\alpha_m(z, t)\}$ by means of the Cayley-Hamilton theorem. We then apply the solution to the single-beam geometry in Section 4 and obtain an analytic expression for the quadrature noise variance. The analytic solution, however, is rather complicated, which prompts us to look at a few simple cases in the second part of this paper in order to obtain some physical insight.

In the second part of this paper, Sections 5 and 6, we consider two extreme limits, namely, that of a short medium and that of an infinitely long medium. The short-medium limit, considered in Section 5, allows us to derive some general rules of thumb as to where (i.e., for what experimental parameters) one may or may never see squeezing. This is because when there is no squeezing in the short-medium limit there will never be any squeezing with an increased medium length. The limit of an infinitely long medium, considered in Section 6, is also important. It demonstrates how an indefinite growth of noise with the medium length can destroy squeezing at most experimental parameters. We show that when the pump-probe phase mismatch is not considered there are only three separate regions where squeezing exists in this limit. There are many more regions with squeezing, however, when the pump-probe phase mismatch is considered. The effect of collisions is also discussed in this limit of an infinitely long medium.

The third part of this paper consists of Sections 7 and 8, where we study the case of a finite medium. In Section 7 we consider the temporally degenerate case and first examine the regions where optimum squeezing is usually obtained, without inclusion of the pump-probe phase mismatch. Then we discuss the effects of the pump-probe phase mismatch, increased pump detuning, Doppler broadening, and Gaussian-intensity variation. It is shown that the pump-probe phase mismatch does not seriously affect the maximum amount of achievable squeezing. Also, we find that Doppler broadening becomes important only when the pump detuning is less than 3 Doppler half-widths from resonance. Moreover, the effect of a Gaussian pump beam can, in general, be summed up as a change in the effective pump intensity except when the intensity begins to saturate the atoms.

The temporally nondegenerate case is considered in Section 8, where we once again discuss the effects of the pump-probe phase mismatch, increased pump detuning, increased pump intensity, and collisions. As in the degenerate case, it is found that the pump-probe phase mismatch does not seriously affect squeezing. Increasing the pump intensity beyond saturation, in this case, may actually help achieve squeezing at higher probe frequencies. Moreover, the effect of collisions is shown to be much less degrading at the nondegenerate frequencies. We also

discuss the effects of Doppler broadening and Gaussian-intensity variation. Below saturation these are similar to the degenerate case. However, when the pump intensity is above saturation the presence of either Doppler broadening or Gaussian-intensity variation or both is shown to have a disastrous effect on the generation of squeezing beyond the generalized Rabi frequency. This occurs even when the pump is detuned far from resonance except when only Doppler broadening is present.

In the fourth part of this paper, Sections 9 and 10, we first consider the problem of self-focusing and defocusing, which turns out to be quite serious. It is shown that self-focusing or defocusing of the pump beam always becomes significant at the medium length at which good squeezing just begins to occur, thus potentially limiting the amount of generated squeezing. The loss of intensity because of self-focusing or defocusing of the pump beam, however, can be made negligible with proper choice of the medium length. A potentially serious problem arises because the focusing or defocusing that is experienced by the pump and probe beams turns out to be quite different. As a result, the squeezed probe modes become phase mismatched from the pump mode as the pump beam propagates farther into the medium.

Finally, in Section 10 we present some general rules of thumb that can be followed to recognize regions where good squeezing can be expected.

2. RECAPITULATION OF PERTINENT RESULTS

In this section we give a self-contained summary of those results in Ref. 2 that are relevant to squeezed-state generation experiments that use forward four-photon mixing.

We are interested in four-photon interactions that involve two strong pump beams at frequency Ω_p , one weak probe beam at frequency Ω_m and another weak probe-conjugate beam (PCB) at frequency $\Omega_{\bar{m}}$. We denote the wave vectors of the pump beams by \vec{k}_{p1}^s and \vec{k}_{p2}^s and those of the probe beams by \vec{k}_m^s and $\vec{k}_{\bar{m}}^s$, respectively. For four-photon mixing to occur, the four beams must satisfy the energy conservation relation $2\Omega_p = \Omega_m + \Omega_{\bar{m}}$ and approximately satisfy the phase-matching condition $\vec{k}_{p1}^s + \vec{k}_{p2}^s = \vec{k}_m^s + \vec{k}_{\bar{m}}^s$. The magnitudes of the beam wave vectors are related to their frequencies by $|\vec{k}_{p1}^s| = |\vec{k}_{p2}^s| = \Omega_p n_p / c$, $|\vec{k}_m^s| = \Omega_m n_m / c$, and $|\vec{k}_{\bar{m}}^s| = \Omega_{\bar{m}} n_{\bar{m}} / c$, where n_p , n_m , and $n_{\bar{m}}$ are the refractive indices seen by the pump, probe, and probe-conjugate beams, respectively.

It is easy to see how the phase-matching condition can in fact be met for the forward four-wave mixing geometry depicted in Fig. 1. ϕ_p denotes the angle between the two pump beams and, similarly, ϕ_b is the angle between the two probe beams. The results in Ref. 2 show that in the nearly degenerate frequency limit the refractive indices seen by the two probe beams are smaller than those seen by the pump beams. Thus for phase matching one must have $\phi_b < \phi_p$. It is then apparent that, as ϕ_p approaches zero, wave coupling without phase mismatch is no longer possible. In particular, this is true when $\phi_p = 0$, i.e., when the two pump beams are spatially degenerate. The results of Ref. 2 also imply that when the two pump beams are spatially degenerate maximum coupling between the two probe beams occurs for $\phi_b = 0$, i.e., when the two

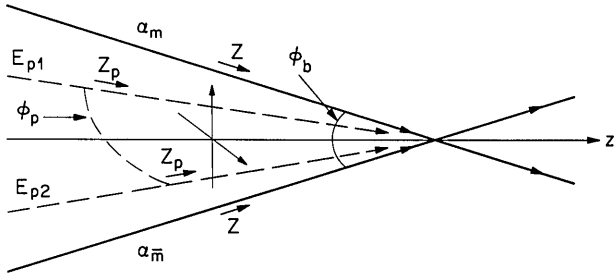


Fig. 1. Geometry of four-wave mixing. In this example the probe beams are depicted by the two solid lines, while the pump beams are the two dashed lines lying in a plane perpendicular to the plane defined by the probe beams. The angle between the probe beams is denoted by ϕ_b , and that between the pump beams is denoted by ϕ_p .

probe beams are spatially degenerate with the pump beams as well. We shall refer to the case in which all four beams are spatially degenerate as the single-beam case.

Let us first consider the situation in which the wave vectors of the four beams are nearly collinear. We define the z axis to be along the line that bisects ϕ_b (see Fig. 1). This enables us to write the c -number variables for the probe beam and PCB electric fields as

$$E_m(Z, t) = \text{Re}\{i\mathcal{E}_m(Z, t)\exp[i(k_m^s Z - \Omega_m t)]\}, \quad (2.1)$$

$$E_{\bar{m}}(Z, t) = \text{Re}\{i\mathcal{E}_{\bar{m}}(Z, t)\exp[i(k_{\bar{m}}^s Z - \Omega_{\bar{m}} t)]\}, \quad (2.2)$$

where Z is the axial coordinate of the wave fronts propagating along the directions of the two probe beams, which can be related to z (the axial coordinate along the z axis) by $Z = z \cos(\phi_b/2)$. \mathcal{E}_m and $\mathcal{E}_{\bar{m}}$ are related to the normalized (c -number) mode amplitudes α_m and $\alpha_{\bar{m}}$ by

$$\mathcal{E}_m(Z, t) = \hbar \tilde{g}_m \alpha_m(Z, t), \quad (2.3)$$

$$\mathcal{E}_{\bar{m}}(Z, t) = \hbar \tilde{g}_{\bar{m}} \alpha_{\bar{m}}(Z, t), \quad (2.4)$$

with $\tilde{g}_m \equiv [(c/v_m)\Omega_m/2\hbar\epsilon_0 A_Q cT]^{1/2}$ and $\tilde{g}_{\bar{m}} \equiv [(c/v_{\bar{m}})\Omega_{\bar{m}}/2\hbar\epsilon_0 A_Q cT]^{1/2}$, where v_m and $v_{\bar{m}}$ are the respective group velocities of the two probe beams. The quantity $A_Q cT$ is the volume of quantization, with cT defining quantization along Z and T chosen to be longer than any time period of interest. We recall that the normalization constants \tilde{g}_m and $\tilde{g}_{\bar{m}}$ are chosen in such a way that the mode-amplitude operators $\hat{\alpha}_m(Z, t)$ and $\hat{\alpha}_{\bar{m}}(Z, t)$ obey the same commutation relations as the usual creation and annihilation operators. The normalization constant \tilde{g}_m , compared with that in the usual field-operator expressions, has an extra c/v_m factor. This extra factor arises because the mode amplitudes are defined in terms of the evenly spaced frequencies $\{\Omega_m\}$ instead of a set of evenly spaced k vectors. The latter would be appropriate if one

were to express the field operators in terms of the usual creation and annihilation operators.

Since all the pertinent equations and the related coefficients are the same for both the probe beam and the PCB except for an interchange of Ω_m with $\Omega_{\bar{m}}$, in the following we will occasionally choose to write the expressions for only one of the two beams.

In our theory the pump beams are treated classically. Also, the z axis will approximately bisect the angle between the two pump beams if the difference between the refractive indices of the two probe beams is small. In such a case we can write the classical electric field of the pump beams as

$$\begin{aligned} E_{p_1}(Z_p, t) &= E_{p_2}(Z_p, t) \\ &= \text{Re}\{i\mathcal{E}_p(Z_p, t)\exp[i(k_p^s Z_p - \Omega_p t)]\}, \end{aligned} \quad (2.5)$$

where $Z_p \equiv z \cos(\phi_p/2) = Z \cos(\phi_p/2)/\cos(\phi_b/2)$. $\mathcal{E}_p(Z_p, t)$, in general, can decay as a function of Z_p . For simplicity we shall consider only the situation in which the pump beams remain undepleted, so that $\mathcal{E}_p(Z_p, t)$ can be approximated by a complex constant $\mathcal{E}_p = |\mathcal{E}_p|\exp(-i\theta_p)$.

In terms of the above definitions, and from the results in Ref. 2, the two probe beams are governed by the following coupled-mode equations:

$$\begin{aligned} \left(\frac{\partial}{\partial Z} + \frac{1}{v_m} \frac{\partial}{\partial t}\right) \alpha_m(Z, t) &= \frac{1}{n_m} [\check{\gamma}_{Rm} \alpha_m(Z, t) \\ &+ \check{X}_m \exp(-i\delta k_m^s Z) \alpha_{\bar{m}}^+(Z, t)] + \check{\Gamma}_m(Z, t), \end{aligned} \quad (2.6)$$

$$\begin{aligned} \left(\frac{\partial}{\partial Z} + \frac{1}{v_{\bar{m}}} \frac{\partial}{\partial t}\right) \alpha_{\bar{m}}^+(Z, t) &= \frac{1}{n_{\bar{m}}} [\check{\gamma}_{R\bar{m}}^* \alpha_{\bar{m}}^+(Z, t) \\ &+ \check{X}_{\bar{m}}^* \exp(i\delta k_{\bar{m}}^s Z) \alpha_m(Z, t)] + \check{\Gamma}_{\bar{m}}^+(Z, t), \end{aligned} \quad (2.7)$$

where δk_m^s , the pump-probe phase mismatch per unit length, is given by $\delta k_m^s = k_m^s + k_{\bar{m}}^s - 2k_p^s \cos(\phi_p/2)/\cos(\phi_b/2)$, and the refractive index $n_m = [1 + (2\check{\gamma}_{Im}c/\Omega_m)]^{1/2}$, with $\check{\gamma}_{Im}$ being the imaginary part of the coefficient $\check{\gamma}_m$ (i.e., $\check{\gamma}_m \equiv \check{\gamma}_{Rm} + i\check{\gamma}_{Im}$). In the general case of four-wave mixing, a transverse intensity grating is formed by the two pump beams. As a result, in order to obtain the coefficients $\check{\gamma}_m$ and \check{X}_m one has to take a spatial average of the atomic polarization over this transverse grating. Such an averaging has been done by Reid and Walls⁴ for the case of degenerate four-wave mixing. The averaging is algebraically more difficult to carry out for the nondegenerate case here. Fortunately, our experimental interest lies mainly in the single-beam case, where no such averaging is necessary. In the following we shall thus concern ourselves with the single-beam case only. For this case the coefficients $\check{\gamma}_m$ and \check{X}_m are given by

$$\begin{aligned} \check{\gamma}_m &= -\frac{\alpha_a(\omega_a/\Omega_m)}{[1 - i(\Delta_p + \delta_m)]\check{S}} \left\{ 1 - \frac{\beta^2}{2\check{S}_{pm} F_{pm}(1 + i\Delta_p)[1 - i(\Delta_p + \delta_m)]} \right\} \\ &\equiv \check{\gamma}_{Rm} + i\check{\gamma}_{Im} \equiv |\check{\gamma}_m| \exp(i\phi_{\check{\gamma}_m}), \end{aligned} \quad (2.8)$$

$$\begin{aligned} \check{X}_m &= \left(\frac{v_m \omega_a^2}{v_{\bar{m}} \Omega_m \Omega_{\bar{m}}}\right)^{1/2} \left(\frac{\alpha_a}{2}\right) \left[\frac{\beta^2 \exp(-2i\theta_p)}{\check{S}_{\bar{m}p} F_{\bar{m}p}(1 - i\Delta_p)[1 - i(\Delta_p + \delta_m)][1 + i(\Delta_p - \delta_m)]} \right] \\ &\equiv \check{X}_{Rm} + i\check{X}_{Im} \equiv |\check{X}_m| \exp(i\phi_{\check{X}_m}), \end{aligned} \quad (2.9)$$

with

$$\tilde{S} = 1 + \frac{\beta^2}{2(1 + \Delta_p^2)}, \quad (2.10)$$

$$F = \frac{\gamma_{\parallel}}{2\gamma_{\perp}}, \quad (2.11)$$

$$\begin{aligned} \tilde{S}_{mp} &= \tilde{S}_{pm}^* = 1 \\ &+ \frac{\beta^2(1 + i\delta_m)}{2F_{mp}[1 - i(\Delta_p - \delta_m)][1 + i(\Delta_p + \delta_m)][1 + i\delta_m/2]} \\ &\equiv \tilde{S}_{Rmp} + i\tilde{S}_{Immp} \equiv |\tilde{S}_{mp}|\exp(i\phi_{\tilde{S}_{mp}}), \end{aligned} \quad (2.12)$$

$$\begin{aligned} F_{mp} &= F_{pm}^* = \frac{1 + i(\delta_m/2F)}{1 + i(\delta_m/2)} \\ &\equiv F_{Rmp} + iF_{Immp} \equiv |F_{mp}|\exp(i\phi_{Fmp}), \end{aligned} \quad (2.13)$$

$$\beta^2 = \frac{16|\mathcal{E}_p|^2|\mu_d|^2}{(\gamma_{\perp}\gamma_{\parallel}/2)\hbar^2(\Omega_p/\omega_a)^2} = \frac{2I_p}{I_{sa}(\Omega_p/\omega_a)^2}, \quad (2.14)$$

$$I_p = 8\epsilon_0 c |\mathcal{E}_p|^2, \quad (2.15)$$

$$I_{sa} = \epsilon_0 c \frac{\gamma_{\perp}\gamma_{\parallel}}{2} \frac{\hbar^2}{|\mu_d|^2}, \quad (2.16)$$

$$\alpha_a = \rho_a |\mu_d|^2 A_{QC} T \mathcal{E}_a^2 / c \gamma_{\perp} = \rho_a |\mu_d|^2 \omega_a / 2\hbar\epsilon_0 c \gamma_{\perp}, \quad (2.17)$$

$$g_a = (\omega_a / 2\hbar\epsilon_0 A_{QC} T)^{1/2}, \quad (2.18)$$

where $\delta_m (= -\delta_{\bar{m}})$ is the frequency detuning of the higher-frequency probe beam from that of the pump beam expressed in terms of the normalized unit set by the transverse relaxation rate γ_{\perp} , i.e., $\delta_m = (\Omega_m - \Omega_p)/\gamma_{\perp}$, $\delta_{\bar{m}} = (\Omega_{\bar{m}} - \Omega_p)/\gamma_{\perp}$, with $\Omega_m > \Omega_p$; Δ_p is the normalized detuning of the pump beam from the atomic resonance frequency ω_a , i.e., $\Delta_p = (\Omega_p - \omega_a)/\gamma_{\perp}$; β is the normalized Rabi frequency; and α_a is the small-signal line-center absorption coefficient. We note that, in arriving at the expression for $\check{\gamma}_m$, we have neglected the contribution to the refractive index from the \hat{A}^2 term in the Hamiltonian. Equation (2.10) gives the expression for the degenerate saturation factor \tilde{S} , while Eq. (2.11) defines the collision factor F , which takes a subunity value when there are collisions. The latter expresses the collisional increase of the atomic transverse relaxation rate γ_{\perp} with respect to the longitudinal relaxation rate γ_{\parallel} . The atomic collisions are assumed to be soft, so that the longitudinal relaxation rate is unperturbed. Equations (2.12) and (2.13) express $\{\tilde{S}_{mp}\}$ and $\{F_{mp}\}$, which can be regarded as the generalized saturation factors and the generalized collision factors, respectively. Equation (2.14) relates β to the pump intensity I_p in terms of the line-center saturation intensity I_{sa} . In the expression for α_a , Eq. (2.17), ρ_a and μ_d are the atomic-number density and the dipole strength, respectively. Finally, in this single-beam case we have taken the combined amplitude of the pump beams to be $2i\mathcal{E}_p$.

For $\delta_m \gg 1$ and $\delta_m - |\Delta_p| \gg 1$, \tilde{S}_{pm} shows a resonance as a function of the probe detuning. In this region, from Eq. (2.12) we see that \tilde{S}_{pm} is approximately zero when $\delta_m = \pm\sqrt{\beta^2 F + \Delta_p^2} \equiv \pm\Delta_R$. This gives rise to a resonance in \check{X}_m and $\check{\gamma}_m$ at $\delta_m = \pm\Delta_R$, which is well studied in the literature, and Δ_R is known as the generalized Rabi frequency. We note that our expressions for $\check{\gamma}_m$ and \check{X}_m coincide with those derived semiclassically in the litera-

ture. For example, it is known that when $F < 1$, $\check{\gamma}_m$ and \check{X}_m display enhanced structure near the degenerate frequency because of coherent population oscillations.⁵ This semiclassical behavior also gives rise to a small enhanced structure in the quantum noise spectra that we studied (see Subsection 8.E).

Note that $\check{\gamma}_m$ can be written in terms of \check{X}_m as

$$\begin{aligned} \check{\gamma}_m &= -\frac{\alpha_a(\omega_a/\Omega_m)}{[1 - i(\Delta_p + \delta_m)]\tilde{S}} \\ &+ \frac{[1 + i(\Delta_p - \delta_m)]\exp(-2i\theta_p)(v_m\Omega_m)^{1/2}}{[1 - i(\Delta_p + \delta_m)](v_{\bar{m}}\Omega_{\bar{m}})^{1/2}}\check{X}_{\bar{m}}^*, \end{aligned} \quad (2.19)$$

which helps us in simplifying the numerical computations. Equations (2.6) and (2.7) tell us that the refractive indices can alter the interaction strengths. In the atomic vapor experiments³ the refractive indices of interest were close to unity. Therefore, in the following, for simplicity we will assume unity refractive indices except when calculating the wave-vector mismatch δk_m^s . Also, since the experiments³ are performed close to the atomic resonance, we shall assume that $(\Omega_m/\omega_a) \approx (\Omega_{\bar{m}}/\omega_a) \approx 1$. We shall further assume that the experiments³ concern a region where the differences among v_m , $v_{\bar{m}}$, and c are negligible. These assumptions can be shown to be valid for the atomic-vapor density of interest to us, even near the generalized Rabi frequency, where the refractive indices are relatively high.

The correlations of the Langevin forces $\{\check{\Gamma}_m(Z)\}$ were obtained in Ref. 2 as follows:

$$\langle \check{\Gamma}_m^+(Z)\check{\Gamma}_n(Z') \rangle = \Lambda_m \delta_{(\delta_m)(\delta_n)} \delta(Z - Z'), \quad (2.20)$$

$$\langle \check{\Gamma}_{\bar{m}}^+(Z)\check{\Gamma}_{\bar{n}}(Z') \rangle = \Lambda_{\bar{m}} \delta_{(\delta_{\bar{m}})(\delta_{\bar{n}})} \delta(Z - Z'), \quad (2.21)$$

$$\begin{aligned} \langle \check{\Gamma}_m(Z)\check{\Gamma}_n(Z') \rangle &= \langle \check{\Gamma}_n(Z)\check{\Gamma}_m(Z') \rangle \\ &= R_m \exp(-2i\theta_p) \delta_{(\delta_m)(-\delta_n)} \\ &\quad \times \exp(-i\delta k_m^s Z) \delta(Z - Z'), \end{aligned} \quad (2.22)$$

$$\begin{aligned} \langle \check{\Gamma}_m^+(Z)\check{\Gamma}_n^+(Z') \rangle &= R_m^* \exp(2i\theta_p) \delta_{(\delta_m)(-\delta_n)} \\ &\quad \times \exp(i\delta k_m^s Z) \delta(Z - Z'), \end{aligned} \quad (2.23)$$

with

$$\Lambda_m = \alpha_a \gamma_{\perp} D_{V_i+V_i}(-\delta_m), \quad (2.24)$$

$$\Lambda_{\bar{m}} = \alpha_a \gamma_{\perp} D_{V_i+V_i}(-\delta_{\bar{m}}), \quad (2.25)$$

$$\begin{aligned} R_m &= R_{\bar{m}} = \alpha_a \gamma_{\perp} D_{V_i+V_i}(-\delta_m) \exp(2i\theta_p) \\ &\equiv R_{Rm} + iR_{Im} \equiv |R_m| \exp(i\phi_{Rm}), \end{aligned} \quad (2.26)$$

$$R_m^* = \alpha_a \gamma_{\perp} D_{V_i+V_i}(-\delta_m) \exp(-2i\theta_p), \quad (2.27)$$

where $\delta_{(\delta_m)(\delta_n)}$ is the Kronecker delta function, which is unity when $\delta_m = \delta_n$ and zero otherwise. In the above equations, $D_{V_i+V_i}(\delta_m)$, $D_{V_i+V_i}(-\delta_m)$, and $D_{V_i+V_i}(\delta_m)$ are given by

$$\begin{aligned} D_{V_i+V_i}(\delta_m) &= \frac{\beta^2 F}{2\gamma_{\perp} D(\delta_m)} \{ (1 - F)[\delta_m^4 + 2\Delta_p \delta_m^3 + \delta_m^2] \\ &\quad \times (4F^2 + 1 - \beta^2 F + \Delta_p^2) - \delta_m \Delta_p \\ &\quad \times (\beta^2 F - 8F^2 - 2\beta^2 F^2) + 4F^2 + \Delta_p^2 \\ &\quad \times (4F^2 + 2\beta^2 F^2) \} + \delta_m^2 \beta^2 F^2 + 4\beta^2 F^2 \\ &\quad + \beta^4 F^2 / 2, \end{aligned} \quad (2.28)$$

$$\begin{aligned}
D_{V_i V_i}(\delta_m) = & -\frac{\beta^2 F}{2\gamma_{\perp} D(\delta_m)} [\exp(-2i\theta_p)] ((1-F) \\
& \times (-\delta_m^2 \beta^2 F + 2\Delta_p^2 \beta^2 F^2) + F\delta_m^4 + \delta_m^2 \\
& \times [4F^3 + F - 3(\Delta_p^2 + \beta^2 F)F] + 4F^3 \\
& + \beta^4 F^2/2 - 12\Delta_p^2 F^3 + i\Delta_p \{(1-F)(-2\beta^2 F^2) \\
& + \delta_m^4 F + \delta_m^2 [4F^3 + 3F - (\Delta_p^2 + \beta^2 F)F] \\
& + 12F^3 - 4\Delta_p^2 F^3\}), \quad (2.29)
\end{aligned}$$

$$D_{V_i + V_i^*}(\delta_m) = D_{V_i V_i^*}(\delta_m), \quad (2.30)$$

$$\begin{aligned}
D(\delta_m) = & (F + \Delta_p^2 F + \beta^2 F/2) \{\delta_m^6 + \delta_m^4 (2 + 4F^2 \\
& - 2\beta^2 F - 2\Delta_p^2) + \delta_m^2 [1 + 8F^2 + 2\beta^2 F \\
& \times (2F - 1) + \beta^4 F^2 + \Delta_p^4 - \Delta_p^2 \\
& \times (8F^2 - 2\beta^2 F - 2)] + 4F^2 + 4\beta^2 F^2 \\
& + \beta^4 F^2 + \Delta_p^2 (8F^2 + 4\beta^2 F^2) + 4\Delta_p^4 F^2\}. \quad (2.31)
\end{aligned}$$

Note that the definitions of $D_{V_i V_i}$ and $D_{V_i + V_i^*}$ are a little different from those in Ref. 2 in that the spatial phase factors are not included in the definitions here. Instead, these factors are accounted for by $\exp(\delta k_m^s Z)$ in Eqs. (2.22) and (2.23). We remind ourselves that although $D_{V_i + V_i^*}(\delta_m)$ and $D_{V_i V_i}(\delta_m)$ are even functions of their argument, $D_{V_i + V_i^*}(\delta_m)$ is not when $F < 1$ and $\Delta_p \neq 0$, which can give rise to an asymmetric spontaneous-emission line shape. Also, in Ref. 2 we used the fact that the delta function $\delta_{(\delta_m)(-\delta_m)}$ implies that $k_n^s = k_{\bar{n}}^s$.

The pump beam obeys the following equation of motion:

$$\left(\frac{\partial}{\partial Z_p} + \frac{1}{v_p} \frac{\partial}{\partial t} \right) \mathcal{E}_p(Z_p, t) = \frac{1}{n_p} \check{\gamma}_{Rp} \mathcal{E}_p(Z_p, t), \quad (2.32)$$

where

$$\begin{aligned}
\check{\gamma}_p = & -\frac{\alpha_a}{[1 - i\Delta_p] \check{S}} \\
\equiv & \check{\gamma}_{Rp} + i\check{\gamma}_{Ip}. \quad (2.33)
\end{aligned}$$

The refractive index n_p seen by the pump beam is given in terms of the imaginary part of $\check{\gamma}_p$ (i.e., $\check{\gamma}_{Ip}$) by means of $n_p = [1 + (2\check{\gamma}_{Ip}c/\Omega_p)]^{1/2}$. It is different from those seen by the probe beams (n_m and $n_{\bar{m}}$) even when the probe-beam frequencies approach that of the pump. Because of this difference in the nonlinear refractive indices seen by the pump and the probe beams, there is a nonzero phase mismatch δk_m^s , which can be expressed as

$$\delta k_m^s = (\Omega_m n_m + \Omega_{\bar{m}} n_{\bar{m}} - 2\Omega_p n_p)/c. \quad (2.34)$$

The presence of such a phase mismatch has also been pointed out by the authors of Ref. 6 for the simple case of a Kerr nonlinearity in an optical fiber.

3. SOLUTION OF COUPLED-MODE EQUATIONS

Consider the following set of coupled-mode equations:

$$\frac{\partial}{\partial Z} b_m(Z) = -\mathcal{R}_m b_m(Z) + \check{X}_m b_{\bar{m}}^+(Z) + G_m(Z), \quad (3.1)$$

$$\frac{\partial}{\partial Z} b_{\bar{m}}^+(Z) = -\mathcal{R}_{\bar{m}}^* b_{\bar{m}}^+(Z) + \check{X}_{\bar{m}}^* b_m(Z) + G_{\bar{m}}^+(Z), \quad (3.2)$$

which can be obtained from Eqs. (2.6) and (2.7) by making the substitutions

$$\begin{aligned}
\mathcal{R}_m = & -\check{\gamma}_{Rm} - i\delta k_m^s/2 \\
\equiv & \mathcal{R}_{Rm} + i\mathcal{R}_{Im} \equiv |\mathcal{R}_m| \exp(i\phi_{\mathcal{R}_m}), \quad (3.3)
\end{aligned}$$

$$b_m(Z) = \alpha_m(Z, t) \exp[i\delta k_m^s Z/2], \quad (3.4)$$

$$G_m(Z) = \check{\Gamma}_m(Z) \exp[i\delta k_m^s Z/2] \quad (3.5)$$

and looking for time-stationary solutions of $\{\alpha_m(Z, t)\}$ by setting the time derivatives of $\{\alpha_m(Z, t)\}$ equal to zero. Since we are interested in solving for $b_m(Z)$ in terms of $b_m(0)$ and $b_{\bar{m}}^+(0)$, let us first write Eqs. (3.1) and (3.2) in matrix form as follows:

$$\frac{\partial}{\partial Z} \bar{B}_m(Z) = \bar{M}_m \bar{B}_m(Z) + \bar{N}_m(Z), \quad (3.6)$$

where

$$\bar{B}_m(Z) \equiv \begin{bmatrix} b_m(Z) \\ b_{\bar{m}}^+(Z) \end{bmatrix}, \quad (3.7)$$

$$\bar{N}_m(Z) \equiv \begin{bmatrix} G_m(Z) \\ G_{\bar{m}}^+(Z) \end{bmatrix}, \quad (3.8)$$

$$\bar{M}_m \equiv \begin{bmatrix} -\mathcal{R}_m & \check{X}_m \\ \check{X}_{\bar{m}}^* & -\mathcal{R}_{\bar{m}}^* \end{bmatrix}. \quad (3.9)$$

Then, formally, the solution of Eq. (3.6) can be written as

$$\bar{B}_m(L) = \exp(\bar{M}_m L) \bar{B}_m(0) + \int_0^L \exp[\bar{M}_m(L - Z')] \bar{N}_m(Z') dZ'. \quad (3.10)$$

In order to evaluate $\exp(\bar{M}_m L)$, we make use of the Cayley-Hamilton theorem, a standard procedure in linear algebra, giving the following solution for the coupled-mode equations (3.1) and (3.2):

$$\begin{aligned}
b_m(L) = & T_m(L) b_m(0) + U_{\bar{m}}(L) b_{\bar{m}}^+(0) \\
& + \int_0^L [T_m(L - Z') G_m(Z') \\
& + U_{\bar{m}}(L - Z') G_{\bar{m}}^+(Z')] dZ', \quad (3.11)
\end{aligned}$$

$$\begin{aligned}
b_{\bar{m}}(L) = & T_{\bar{m}}(L) b_{\bar{m}}(0) + U_m(L) b_m^+(0) \\
& + \int_0^L [T_{\bar{m}}(L - Z') G_{\bar{m}}(Z') \\
& + U_m(L - Z') G_m^+(Z')] dZ', \quad (3.12)
\end{aligned}$$

where

$$T_m(Z) = \exp(-S_m Z) [Q_m \sinh(W_m Z) + \cosh(W_m Z)], \quad (3.13)$$

$$U_{\bar{m}}(Z) = \exp(-S_m Z) [(X_m/W_m) \sinh(W_m Z)], \quad (3.14)$$

with

$$\begin{aligned}
S_m = & (\mathcal{R}_m + \mathcal{R}_{\bar{m}}^*)/2 \\
= & -(\check{\gamma}_{Rm} + \check{\gamma}_{R\bar{m}})/2 \\
\equiv & S_{Rm} + iS_{Im} \equiv |S_m| \exp(i\phi_{S_m}), \quad (3.15)
\end{aligned}$$

$$\begin{aligned}
Q_m &= -Q_{\bar{m}}^* = (\mathcal{R}_m - \mathcal{R}_{\bar{m}}^*)/2W_m \\
&= (-\check{\gamma}_{Rm} + \check{\gamma}_{R\bar{m}} - i\delta k_m^s)/2W_m \\
&\equiv Q_{Rm} + iQ_{Im} \equiv |Q_m|\exp(i\phi_{Q_m}), \quad (3.16)
\end{aligned}$$

$$\begin{aligned}
W_m &= W_{\bar{m}}^* = \left[\left(\frac{\mathcal{R}_{\bar{m}}^* - \mathcal{R}_m}{2} \right)^2 + (\check{X}_{\bar{m}}^* \check{X}_m) \right]^{1/2} \\
&= \left[\left(\frac{-\check{\gamma}_{Rm} + \check{\gamma}_{R\bar{m}} - i\delta k_m^s}{2} \right)^2 + (\check{X}_{\bar{m}}^* \check{X}_m) \right]^{1/2} \\
&\equiv W_{Rm} + iW_{Im} \equiv |W_m|\exp(i\phi_{W_m}). \quad (3.17)
\end{aligned}$$

4. SINGLE-BEAM CASE

In squeezed-state generation experiments using four-wave mixing, if the probe beam and the PCB at the input are in their vacuum states, then a squeezed-vacuum state can be obtained by combining the two at the output with a 50/50 beam splitter.⁷ In the single-beam configuration considered here, the geometry has the probe beam and the PCB combined already at the output, so no 50/50 beam splitter is needed. Since the pump beam also comes out together with the probe beam and the PCB, with its frequency between those of the probe beam and the PCB, the pump beam can potentially be used as a local oscillator (LO) for phase-sensitive heterodyne detection of the field fluctuations in the generated squeezed vacuum. However, as explained below, the phase of the pump beam is in general not of the correct value for the observation of nonclassical reduction of the photocurrent noise.

One sees squeezing as a result of parametric deamplification of the vacuum-field fluctuations through some nonlinear optical interaction that is caused by a strong pump beam. Because of energy conservation, it is impossible for the pump beam to reduce its own amplitude by deamplifying itself. In other words, near the degenerate frequency the quadrature whose vacuum-field fluctuations are reduced cannot possibly coincide with that of the pump. Thus the transmitted pump beam is always at the wrong phase for observation of nonclassical photocurrent fluctuations near the zero frequency. It also turns out that the LO phase that is required for observation of sub-shot-noise photocurrent fluctuations varies slowly with the photocurrent frequency. Therefore the transmitted pump phase is not of the right value for observation of squeezing at nondegenerate probe frequencies either. Thus, in general, if one wants to observe the nonclassical photocurrent fluctuations, one must either remove the pump beam and reintroduce a LO beam with the right phase or resort to some external means of shifting the pump-beam phase.³ This pump-phase problem is also encountered in squeezed-state generation experiments using optical fibers.⁶

To obtain the quadrature noise that is picked up by a homodyne detector, we take the LO field $E_{LO}(Z, t)$ to be

$$E_{LO}(Z, t) = \text{Re}\{i|\mathcal{E}_{LO}|\exp(-i\theta_{LO})\exp[i(k_p^s Z - \Omega_p t)]\}, \quad (4.1)$$

where θ_{LO} is the absolute phase of the LO and we have taken its frequency to be equal to that of the pump. The generated photocurrent operator $\hat{I}(t)$ is proportional to $\hat{A}^\dagger(t)\hat{A}(t)$, and $\hat{A}(t)$ is in turn proportional to the probe field at the output of the medium; i.e., $\hat{A}(t) \propto \sum_m \hat{\alpha}_m(L, t) \times$

$\exp[i(k_m^s L - \Omega_m t)]$, where L is the length of the medium. Denoting the Fourier transform of $\hat{I}(t)$ at frequency $\Omega_m - \Omega_p$ by \hat{I}_m , we can show the variance $\langle \hat{I}_m^\dagger \hat{I}_m \rangle$ to be proportional to

$$\begin{aligned}
\delta X^1(\theta) &= 1/4 + 1/4[\langle \hat{\alpha}_m^\dagger(L)\hat{\alpha}_m(L) \rangle + \langle \hat{\alpha}_{\bar{m}}^\dagger(L)\hat{\alpha}_{\bar{m}}(L) \rangle \\
&\quad + \langle \hat{\alpha}_m(L)\hat{\alpha}_{\bar{m}}(L) \rangle \exp(2i\theta_{LO}) \\
&\quad + \langle \hat{\alpha}_m^\dagger(L)\hat{\alpha}_{\bar{m}}^\dagger(L) \rangle \exp(-2i\theta_{LO})], \quad (4.2)
\end{aligned}$$

where we have assumed time stationarity and thus omitted the time variable. We shall refer to $\delta X^1(\theta)$ as the normalized quadrature noise. $\delta X^1(\theta)$ can be shown to be dependent only on the difference between the phases of the pump and the LO, which we denote as θ ; i.e., $\theta \equiv \theta_{LO} - \theta_p$. When the modes $\{\hat{\alpha}_m(L)\}$ are in their vacuum states, the value of $\delta X^1(\theta)$ will be 1/4, giving the usual shot-noise level. On the other hand, when the modes $\{\hat{\alpha}_m(L)\}$ are in squeezed-vacuum states, the value of $\delta X^1(\theta)$ can fall below 1/4 for some value of θ . Since the c -number variables have been obtained by normal ordering, their correlations directly give the normally ordered operator correlations in Eq. (4.2).

For each set of experimental parameters the value of $\delta X^1(\theta)$ can always be minimized for a particular value of θ to yield the maximum amount of squeezing. This particular value of θ will be denoted as θ_{\min} . If we further denote the percentage of maximum squeezing by $\mathcal{S} \times 100\%$, then

$$\mathcal{S} \equiv 1 - 4\delta X^1(\theta_{\min}). \quad (4.3)$$

Moreover, if θ is changed to $\theta + \pi/2$, the photocurrent noise is maximized; i.e., the maximally desqueezed quadrature is observed instead of the maximally squeezed quadrature. This maximum noise is also a quantity that can be observed experimentally. It can be expressed in terms of the percentage of photocurrent-noise enhancement over the shot-noise level. Denoting the percentage of maximum noise enhancement by $\mathcal{N} \times 100\%$, we get

$$\mathcal{N} \equiv 4\delta X^1(\theta_{\min} + \pi/2) - 1. \quad (4.4)$$

To calculate $\delta X^1(\theta)$, we need the various correlations of $\alpha_m(L)$, which can be obtained by using Eqs. (3.4), (3.5), (3.11), and (3.12). To illustrate the method, consider the correlation $\langle \alpha_m(L)\hat{\alpha}_{\bar{m}}(L) \rangle$. From Eqs. (3.4), (3.5), (3.11), and (3.12), we see that it contains a term of the form

$$\begin{aligned}
&\left\langle \int_0^L dZ' \int_0^L dZ'' T_m(L - Z') G_m(Z') T_{\bar{m}}(L - Z'') G_{\bar{m}}(Z'') \right\rangle \\
&\quad \times \exp(-i\delta k_m^s L) = \int_0^L dZ' \int_0^L dZ'' T_m(L - Z') T_{\bar{m}}(L - Z'') \\
&\quad \times \exp(i\delta k_m^s Z'/2 + i\delta k_{\bar{m}}^s Z''/2) \langle \check{\Gamma}_m(Z') \check{\Gamma}_{\bar{m}}(Z'') \rangle \\
&\quad \times \exp(-i\delta k_m^s L) \\
&= R_m \exp(-2i\theta_p) \exp(-i\delta k_m^s L) \int_0^L dZ' T_m(L - Z') T_{\bar{m}}(L - Z'), \quad (4.5)
\end{aligned}$$

which is easily evaluated because the integral $\int_0^L dZ' \times L_m(Z - Z') L_{\bar{m}}(Z - Z')$ involves only exponential functions [see Eq. (3.13)]. The other terms in $\langle \alpha_m(L)\alpha_{\bar{m}}(L) \rangle$ and the

remaining correlations entering Eq. (4.2) can be calculated in a similar manner. We note that many correlations, such as $\langle G_m(Z')G_m(Z'') \rangle$, are zero, which simplifies the calculations somewhat. The results can be summarized as follows:

$$\begin{aligned} \langle \alpha_m^+(L)\alpha_m(L) \rangle &= \Lambda_m^+ I_{T_m^* T_m} + R_m^* \exp(2i\theta_p) I_{T_m^* U_{\bar{m}}} \\ &+ \Lambda_{\bar{m}} I_{U_{\bar{m}}^* U_{\bar{m}}} + R_m \exp(-2i\theta_p) I_{U_{\bar{m}}^* T_m}, \end{aligned} \quad (4.6)$$

$$\begin{aligned} \langle \alpha_{\bar{m}}^+(L)\alpha_{\bar{m}}(L) \rangle &= \Lambda_{\bar{m}} I_{T_{\bar{m}}^* T_{\bar{m}}} + R_m^* \exp(2i\theta_p) I_{T_{\bar{m}}^* U_m} \\ &+ \Lambda_m I_{U_m^* U_m} + R_m \exp(-2i\theta_p) I_{U_m^* T_{\bar{m}}}, \end{aligned} \quad (4.7)$$

$$\begin{aligned} \langle \alpha_m(L)\alpha_{\bar{m}}(L) \rangle &= \exp(-i\delta k_m^s L) [R_m \exp(-2i\theta_p) I_{T_m T_{\bar{m}}} \\ &+ \Lambda_m I_{T_m U_m} + R_m^* \exp(2i\theta_p) I_{U_{\bar{m}} U_m} \\ &+ \Lambda_{\bar{m}} I_{U_{\bar{m}} T_{\bar{m}}}], \end{aligned} \quad (4.8)$$

$$\begin{aligned} \langle \alpha_m^+(L)\alpha_{\bar{m}}^+(L) \rangle &= \exp(i\delta k_m^s L) [R_m^* \exp(2i\theta_p) I_{T_m^* T_{\bar{m}}^*} \\ &+ \Lambda_m I_{T_m^* U_m^*} + R_m \exp(-2i\theta_p) I_{U_{\bar{m}}^* U_m^*} \\ &+ \Lambda_{\bar{m}} I_{U_{\bar{m}}^* T_{\bar{m}}^*}], \end{aligned} \quad (4.9)$$

where

$$I_{T_m T_{\bar{m}}} \equiv \int_0^L dZ T_m(Z) T_{\bar{m}}(Z), \quad (4.10)$$

$$I_{T_m U_m} \equiv \int_0^L dZ T_m(Z) U_m(Z), \quad (4.11)$$

etc. From Eqs. (2.8), (2.9), (3.13), and (3.14), we note that U_m is proportional to $\exp(-2i\theta_p)$, while T_m is independent of θ_p . Thus it is clear that $\langle \alpha_m(L)\alpha_{\bar{m}}(L) \rangle \propto \exp(-2i\theta_p)$ and $\langle \alpha_m^+(L)\alpha_m(L) \rangle$ is independent of θ_p . This shows that δX^1 is indeed dependent only on θ , as was mentioned above.

By explicitly evaluating the integrals in Eqs. (4.6)–(4.9), we obtain

$$\begin{aligned} I_{T_m^* T_m} &= Q_m^* Q_m (U_{m+} + U_{m-} - A_{m+} - A_{m-}) \\ &+ Q_m^* (-U_{m+} + U_{m-} + A_{m+} - A_{m-}) \\ &+ Q_m (-U_{m+} + U_{m-} - A_{m+} + A_{m-}) \\ &+ (U_{m+} + U_{m-} + A_{m+} + A_{m-}), \end{aligned} \quad (4.12)$$

$$\begin{aligned} I_{T_{\bar{m}} T_m} &= Q_{\bar{m}} Q_m (U_{m+} + U_{m-} - A_{m+} - A_{m-}) \\ &+ Q_{\bar{m}} (-U_{m+} + U_{m-} + A_{m+} - A_{m-}) \\ &+ Q_m (-U_{m+} + U_{m-} - A_{m+} + A_{m-}) \\ &+ (U_{m+} + U_{m-} + A_{m+} + A_{m-}), \end{aligned} \quad (4.13)$$

$$\begin{aligned} I_{T_m^* U_m} &= Q_m^* (\check{X}_m/W_m) (U_{m+} + U_{m-} - A_{m+} - A_{m-}) \\ &+ \frac{\check{X}_m}{W_m} (-U_{m+} + U_{m-} - A_{m+} + A_{m-}), \end{aligned} \quad (4.14)$$

$$\begin{aligned} I_{T_{\bar{m}} U_m} &= Q_{\bar{m}} \frac{\check{X}_m}{W_m} (U_{m+} + U_{m-} - A_{m+} - A_{m-}) \\ &+ \frac{\check{X}_m}{W_m} (-U_{m+} + U_{m-} - A_{m+} + A_{m-}), \end{aligned} \quad (4.15)$$

$$I_{U_m^* U_m} = \frac{\check{X}_m^* \check{X}_m}{W_m^* W_m} (U_{m+} + U_{m-} - A_{m+} - A_{m-}), \quad (4.16)$$

$$I_{U_{\bar{m}} U_m} = \frac{\check{X}_{\bar{m}} \check{X}_m}{W_{\bar{m}} W_m} (U_{m+} + U_{m-} - A_{m+} - A_{m-}), \quad (4.17)$$

with

$$U_{m+} = \frac{1 - \exp(-\mu_{m+} L)}{4\mu_{m+}}, \quad (4.18)$$

$$U_{m-} = \frac{1 - \exp(-\mu_{m-} L)}{4\mu_{m-}}, \quad (4.19)$$

$$A_{m+} = \frac{1 - \exp(-\alpha_{m+} L)}{4\alpha_{m+}}, \quad (4.20)$$

$$A_{m-} = \frac{1 - \exp(-\alpha_{m-} L)}{4\alpha_{m-}}, \quad (4.21)$$

and

$$\mu_{m+} = 2S_{Rm} + 2W_{Rm}, \quad (4.22)$$

$$\mu_{m-} = 2S_{Rm} - 2W_{Rm}, \quad (4.23)$$

$$\alpha_{m+} = 2S_{Rm} + 2iW_{Im}, \quad (4.24)$$

$$\alpha_{m-} = 2S_{Rm} - 2iW_{Im}, \quad (4.25)$$

where S_{Rm} , W_{Rm} , and W_{Im} are defined in Eqs. (3.15) and (3.17). The remaining integrals can be obtained from those given in Eqs. (4.12)–(4.17) by complex conjugation. For example, $I_{T_{\bar{m}}^* T_m^*}$ is just the complex conjugate of $I_{T_{\bar{m}} T_m}$. The final expression for $\delta X^1(\theta)$ turns out to be dependent on the medium length by the dimensionless quantity $\alpha_a L$, which is the length of the medium normalized by the line-center absorption length $1/\alpha_a$. For convenience, in the following we shall denote $\alpha_a L$ by L_a .

5. SHORT-MEDIUM LIMIT

We have seen in Section 4 that the analytic solution for the quadrature-noise variance is rather complicated. Nevertheless, important information as to where one may find squeezing can be obtained by studying the simple case of a short medium, i.e., the case with $L_a \ll 1$. In this limit the solution, as given through Eqs. (3.11) and (3.12), of the coupled-mode equations (3.1) and (3.2) is simplified a great deal, yielding

$$\alpha_m(L, t) = \check{\gamma}_{Rm} \alpha_m(0, t) L + \check{X}_m \alpha_{\bar{m}}^+(0, t) L + \check{\Gamma}_m(0, t) L. \quad (5.1)$$

When the input beams are all in their vacuum states, the correlations among

$$\{\alpha_m(0, t), \alpha_{\bar{m}}^+(0, t)\}$$

will all be zero. This is because we are working with normally ordered c -number variables. The correlations among $\{\alpha_m(L, t), \alpha_{\bar{m}}^+(L, t)\}$ will then depend only on the correlations among the Langevin forces $\{\check{\Gamma}_m(Z=0), \check{\Gamma}_{\bar{m}}^+(Z=0)\}$. In this case Eqs. (5.1) and (4.2) give

$$\begin{aligned} \delta X^1(\theta) &= \frac{1}{4} + \frac{L^2}{4} [\Lambda_m + \Lambda_{\bar{m}} + |R_m| \exp(i\phi_{Rm}) \exp(i2\theta) \\ &+ |R_m| \exp(-i\phi_{Rm}) \exp(-i2\theta)], \end{aligned} \quad (5.2)$$

which tells us that $\delta X^1(\theta)$ can be minimized by choosing $\theta = \theta_{\min}$, where

$$\theta_{\min} = (-\phi_{Rm} + \pi)/2; \quad (5.3)$$

this step leads to the following minimum quadrature noise:

$$\delta X^1(\theta_{\min}) = \frac{1}{4} + \frac{L^2}{4}(\Lambda_m + \Lambda_{\bar{m}} - 2|R_m|). \quad (5.4)$$

The quadrature noise $\delta X^1(\theta_{\min})$ will fall below the classical value of 1/4 only if the term $(\Lambda_m + \Lambda_{\bar{m}} - 2|R_m|)$ is negative. The condition for observing squeezing in a short medium is thus

$$\Lambda_m + \Lambda_{\bar{m}} - 2|R_m| < 0. \quad (5.5)$$

A. Degenerate Case

In the degenerate-frequency limit (i.e., $m = 0$), without consideration of the atomic collisions ($F = 1$), Eqs. (2.24)–(2.31) reduce to

$$\Lambda_0 = \frac{\alpha_a \beta^2 [4\beta^2 + (\beta^4/2)]}{8(1 + \Delta_p^2)^3 \bar{S}^3}, \quad (5.6)$$

$$R_{R0} = \frac{-\alpha_a \beta^2 [4 + (\beta^4/2) - 12\Delta_p^2]}{8(1 + \Delta_p^2)^3 \bar{S}^3}, \quad (5.7)$$

$$R_{I0} = \frac{-\alpha_a \beta^2 [12\Delta_p - 4\Delta_p^3]}{8(1 + \Delta_p^2)^3 \bar{S}^3}. \quad (5.8)$$

Furthermore, when $\beta \gg 1$ and $\Delta_p \gg 1$, the short-medium squeezing condition $\Lambda_0^2 < R_{I0}^2 + R_{R0}^2$ [inequality (5.5) with $m = 0$] will be satisfied if

$$4\Delta_p^6 > 3\beta^4 \Delta_p^2 + \beta^6. \quad (5.9)$$

Equality prevails in (5.9) when $\Delta_p = \pm\beta$, which implies that inequality (5.9) can be reduced to

$$|\Delta_p| > \beta. \quad (5.10)$$

Defining $\beta_c \equiv |\Delta_p|$, the above discussion tells us that if the pump intensity exceeds a certain value so that $\beta > \beta_c$, then there will be no squeezing at the degenerate frequency. Physically this is caused by the deteriorating effect of spontaneous emission by the atoms when they become highly excited.⁴ Since at a detuning Δ_p intensity saturation of the absorption coefficient occurs for $\beta^2 > 2\Delta_p^2$, we conclude that for squeezing to be observed at the degenerate frequency, intensity saturation of the atomic absorption must be avoided. Such is not the case at nondegenerate frequencies, as is shown in Subsection 8.D below.

Spontaneously emitted light has a frequency width that is of the order of γ_{\parallel} . Thus, although there is no squeezing at $\delta_m = 0$ when $\beta > \beta_c$, one may still expect to see squeezing if the photocurrent noise is observed at a frequency far enough from zero. This brings us to consider the nondegenerate-frequency case.

B. Nondegenerate Case

From Eqs. (2.24)–(2.31), at nondegenerate frequencies with $F = 1$, one has

$$\begin{aligned} \Lambda_m &= \Lambda_{\bar{m}} \\ &= \frac{(-\alpha_a \beta^2) [4\beta^2 + (\beta^4/2) + \delta_m^2 \beta^2]}{2D(\delta_m)|_{F=1}}, \end{aligned} \quad (5.11)$$

$$R_{Im} = \frac{(-\alpha_a \beta^2) [12\Delta_p - 4\Delta_p^3 + \delta_m^2 \Delta_p (7 - \Omega_R^2) + \delta_m^4 \Delta_p]}{2D(\delta_m)|_{F=1}}, \quad (5.12)$$

$$R_{Rm} = \frac{(-\alpha_a \beta^2) [4 + (\beta^4/2) - 12\Delta_p^2 + \delta_m^2 (5 - 3\Omega_R^2) + \delta_m^4]}{2D(\delta_m)|_{F=1}}, \quad (5.13)$$

where $D(\delta_m)$ is given by Eq. (2.31). Once again, by evaluating inequality (5.5) in the limit where $\beta > \Delta_p \gg 1$ and $\delta_m \ll \beta$, we get

$$\begin{aligned} &\delta_m^4 \Delta_p^2 \Delta_R^4 + \delta_m^2 [(8\Delta_p^4 - 3\beta^4) \Delta_R^2 - \beta^6] \\ &> 4\Delta_p^2 (3\beta^4 - 4\Delta_p^4) + 4\beta^6, \end{aligned} \quad (5.14)$$

which is the condition for observing squeezing in a short medium at nondegenerate frequencies. The above inequality can be further simplified in the following two cases. The first is when β is just above the critical value β_c ; i.e., $\beta \geq |\Delta_p|$. In this case inequality (5.5) can be met with $\delta_m < 1$, enabling us to neglect the δ_m^4 term in Eq. (5.14) to give

$$\begin{aligned} \delta_m^2 &> \frac{4\Delta_p^2 (3\beta^4 - 4\Delta_p^4) + 4\beta^6}{(8\Delta_p^4 - 3\beta^4) \Delta_R^2 - \beta^6} \\ &= \frac{4\Delta_p^2 (3\beta^4 - 4\Delta_p^4) + 4\beta^6}{9\beta^6}. \end{aligned} \quad (5.15)$$

Second, when $\beta^2 \gg 3\Delta_p^2$, terms of order Δ_p^2 in inequality (5.14) become negligible compared with terms of order β^2 . In this case inequality (5.14) reduces to

$$\delta_m^4 - \delta_m^2 \frac{4\beta^2}{\Delta_p^2} > \frac{4\beta^2}{\Delta_p^2}. \quad (5.16)$$

Furthermore, by solving for δ_m^2 with the above inequality replaced by an equality, we can show that under the condition that $\beta^2 \geq 3\Delta_p^2$, inequality (5.16) becomes

$$\delta_m^2 > \frac{4\beta^2}{\Delta_p^2}. \quad (5.17)$$

We define δ_c^2 ($\delta_c > 0$) to be equal to the right-hand side of inequality (5.15) or (5.17), whichever is relevant. The above derivation then tells us that with $\beta > \beta_c$ squeezing can always be observed if one looks at a frequency far enough from degeneracy that $\delta_m > \delta_c$.

The two quantities, β_c and δ_c , tell everything that we want to know about the possibility of observing squeezing in a short medium. In order to achieve a large amount of squeezing, however, it is still necessary to go to the limit of a long medium. When there is no squeezing in the short-medium limit, there will never be any squeezing in a long medium either. Hence, despite some other complications that arise in the case of a long medium, the discussion here provides some simple rules of thumb to follow in order to find regions where one may or may never see squeezing.

6. INFINITELY LONG MEDIUM LIMIT

Before considering the more realistic case of a long, but finite, medium, let us first look at the simpler behavior of

an infinitely long medium for which $L \rightarrow \infty$. Although this case is physically unrealistic, important insights can be obtained by analyzing this limit. We shall make comparisons with the results of the degenerate theory of Reid and Walls,⁴ which also assumes an infinitely long medium. For simplicity, we shall neglect Doppler broadening and Gaussian-intensity variation, deferring their discussion until Section 7.

What happens when $L \rightarrow \infty$? In this limit the factors U_{m+} , A_{m+} , and A_{m-} in $\delta X^1(\theta)$ achieve some finite values [see Eqs. (4.18)–(4.21)]. However, as noted by Reid and Walls,⁴ the factor U_{m-} of Eq. (4.19) can become unbounded. Such would be the case if μ_{m-} were negative or, from Eq. (4.23), if $S_{Rm} < W_{Rm}$. In this situation squeezing could occur only at those phase angles θ at which all the exponentially unbounded terms in $\delta X^1(\theta)$ somehow cancel one another.

To examine conditions under which such a cancellation occurs, we decompose $\delta X^1(\theta)$ of Eq. (4.2) into one part $\delta E(\theta)$ that depends on $\exp(-\mu_{m-}L)$ and another part $\delta N(\theta)$ that does not. We can then write

$$\delta X^1(\theta) = \delta N(\theta) + \delta E(\theta), \quad (6.1)$$

with

$$\delta E(\theta) \equiv [E_{Rm} + E_{Cm} \exp(2i\theta - i\delta k_m^s L) + E_{Cm}^* \exp(-2i\theta + i\delta k_m^s L)] \exp(-\mu_{m-}L), \quad (6.2)$$

where E_{Rm} is real, E_{Cm} is complex, and both E_{Rm} and E_{Cm} are independent of θ . In order for the potentially growing part $\delta E(\theta)$ to vanish, Eq. (6.2) tells us that θ must be chosen according to

$$\theta = [\cos^{-1}(\zeta_m) - \phi_{E_{Cm}} + \delta k_m^s L]/2, \quad (6.3)$$

where

$$\zeta_m = -\frac{E_{Rm}}{2|E_{Cm}|} \quad (6.4)$$

and we have defined $E_{Cm} \equiv |E_{Cm}| \exp(i\phi_{E_{Cm}})$. The arc-cosine term in Eq. (6.3), however, has a real value only if

$$|\zeta_m| \leq 1. \quad (6.5)$$

In other words, $\delta E(\theta)$ can be zero only if inequality (6.5) is satisfied. Thus, for stability in the growth of noise as $L \rightarrow \infty$, we have two conditions of concern. We call the condition

$$\mu_{m-} > 0 \quad (6.6)$$

the stability-rate condition and that of Eq. (6.5) the stability-phase condition. The above analysis tells us that when the stability-rate condition is violated, there will be an unstable growth of noise for all values of θ , with the possible exception of one (two) particular value(s) that would exist if the stability-phase condition were also satisfied with equality (inequality). Physically, the infinite noise growth in some phase quadrature occurs because of our assumption that the pump beam is not depleted. As a result, if the loss S_{Rm} is low, in the $L \rightarrow \infty$ limit the pump beam can dump an infinite amount of energy into some quadrature of the probe beams. This could occur through either parametric amplification or spontaneous emission.

A. Degenerate Case without Atomic Collisions

We first apply the above results to the degenerate-frequency case with the assumption that there are no atomic collisions (i.e., $m = 0$ and $F = 1$), for comparison with the degenerate theory of Reid and Walls.⁴ At the end of this subsection we shall examine the ideal-noise limit where the pump beam is detuned far from the atomic resonance. We shall also discuss the effect of pump-probe phase mismatch, which was not accounted for in the theory given by Reid and Walls.⁴

In this simple degenerate-frequency case, the various coefficients and correlations given by Eqs. (2.8)–(2.18) and (2.24)–(2.31) reduce to

$$\check{\gamma}_0 = -\frac{\alpha_a(1 + i\Delta_p)}{\tilde{S}^2(1 + \Delta_p^2)}, \quad (6.7)$$

$$\check{X}_0 = \frac{\alpha_a\beta^2}{2(1 - i\Delta_p)\tilde{S}^2(1 + \Delta_p^2)}, \quad (6.8)$$

$$\tilde{S} = 1 + \frac{\beta^2}{2(1 + \Delta_p^2)}, \quad (6.9)$$

with Λ_0 , R_{R0} , and R_{I0} as in Eqs. (5.6)–(5.8). We note that the above coefficients are slightly different from those given by Reid and Walls.⁴ This is because of some extra terms that arise in the expressions for $\check{\gamma}_0$ and \check{X}_0 in our single-beam geometry, which are otherwise negligible in the usual four-wave mixing geometry because of phase mismatching (see Ref. 2).

It can be shown that in the degenerate-frequency limit, where $\check{\gamma}_{Rm} = \check{\gamma}_{R\bar{m}}$ and $\check{X}_m = X_{\bar{m}}$, Q_m of Eq. (3.16) becomes purely imaginary. Furthermore, we have verified by an explicit algebraic calculation that whenever Q_m becomes imaginary the stability-phase condition (6.5) is satisfied with equality. This implies that in the degenerate-frequency limit there exists only one value of θ for which the exponentially growing part in Eq. (6.1) can be nulled. However, as one detunes away from degeneracy, the loss coefficients $\check{\gamma}_{Rm}$ and $\check{\gamma}_{R\bar{m}}$ become unequal, imparting a real part to Q_m . Numerical evaluation then shows that the stability-phase condition is violated as one detunes ever so slightly from degeneracy. Therefore, near the degenerate frequency, the region where the stability-phase condition can be satisfied is a line of measure zero in the parameter space. As we shall point out below, at nondegenerate frequencies there is another line of measure zero where the stability-phase condition can be satisfied.

In the degenerate-frequency limit we can show that $\phi_{E_{C0}} = \phi_{\check{x}_0}$. Thus the stability-phase condition, Eq. (6.3), becomes

$$2\theta = \cos^{-1}(-1) - \phi_{\check{x}_0} + \delta k_0^s L \\ = \pi - \phi_{\check{x}_0} + \delta k_0^s L. \quad (6.10)$$

This implies that, if the stability-rate condition is violated so that U_{0-} of Eq. (4.19) becomes unbounded, then for squeezing to be achieved the value of θ_{\min} must be given by

$$\theta_{\min} = (\pi - \phi_{\check{x}_0} + \delta k_0^s L)/2. \quad (6.11)$$

Furthermore, to compare our results with those of Reid and Walls,⁴ where the pump-probe phase mismatch is not considered, we arbitrarily set $\delta k_0^s = 0$. The above ex-

pression for θ_{\min} then agrees with the statement of Reid and Walls that $\cos(2\theta_{\min}) = -\check{X}_{R0}/|\check{X}_0|$. Moreover, the stability-rate condition is violated only when β^2 exceeds a certain value, which from Eqs. (3.15), (3.17), (4.23), and (6.7)–(6.9) and inequality (6.6) is given by

$$\beta^2 > 2(1 + \Delta_p^2)^{1/2}. \quad (6.12)$$

When that happens, the following expression for the minimum-phase quadrature noise (with $\delta k_m^s = 0$) is easily obtained:

$$\delta X^1(\theta_{\min}) = \frac{1}{4} + \frac{\Lambda_0 |\check{X}_0| - (R_{R0} \check{X}_{R0} + R_{I0} \check{X}_{I0})}{4 |\check{X}_0| (\check{\gamma}_{R0} + |\check{X}_0|)}. \quad (6.13)$$

On the other hand, when the stability-rate condition is satisfied the minimum-phase quadrature noise is not necessarily given by the above equation, because θ_{\min} no longer obeys the simple expression of Eq. (6.11). In this case we resort to numerical methods to find the value of $\delta X^1(\theta_{\min})$.

We note that θ_{\min} of Eq. (6.11) is different from that given by Eq. (5.3) for the short-medium limit. This is because \check{X}_0 is generally different from R_0 close to the atomic resonance. So, when the stability-rate condition is violated, the squeezing behavior as $L \rightarrow \infty$ can, in general, be quite different from that exhibited in the short-medium limit. In particular, the range of β values with squeezing in the long-medium limit may be smaller than that in the short-medium limit. However, \check{X}_0 can approach R_0 , as it does in the ideal-noise situation described below.

The ideal-noise situation occurs when the atom-field interaction can be described by a simple quadratic Hamiltonian with the inclusion of an ideal-loss mechanism, as discussed by Kumar and Shapiro.⁸ In the c -number-variable formulation here, one approaches the ideal-noise situation when the following two conditions are satisfied: $R_0 = iR_{I0} = \check{X}_0$ and $|\Lambda_0| \ll |R_0|$. If we consider the region where $|\Delta_p| > 3$ and $\beta > 3$, then these two conditions can be satisfied with $2\Delta_p^2 > \beta^2$ and $|\Delta_p^3| > \beta^4/8$. As correctly pointed out by Reid and Walls,⁴ outside the ideal-noise region the dominant noise that reduces squeezing is that from spontaneous emission and not the back-action noise caused by the presence of loss. In the ideal-noise region, Eq. (6.13) simplifies to

$$\delta X^1(\theta_{\min}) = \frac{1}{4} - \frac{|\check{X}_0|}{4(\check{\gamma}_{R0} + |\check{X}_0|)}. \quad (6.14)$$

The effect of loss on squeezing can be divided into a relatively lossy region and a relatively lossless region. In fact, the stability-rate condition provides a convenient way to make this division because it is satisfied only when the medium is relatively lossy (and vice versa). From Eq. (6.12) we then find that the atomic medium is relatively lossy when $\beta^2 < 2|\Delta_p|$. As pointed out by Kumar and Shapiro,⁸ in this region the amount of squeezing is basically limited by the ratio $|\check{X}_0|/\check{\gamma}_{R0}$, which can also be seen from Eq. (6.14). Thus we can expect to achieve good squeezing when both the ideal-noise condition and the relatively lossless condition are satisfied.

We now illustrate the above discussion with some examples that plot the amount of squeezing \mathcal{S} . A convenient format is to plot $1 - \mathcal{S}$ as a function of β , which will be

called the squeezing-intensity plot. Below, we shall often compare and contrast two situations, one in which the pump-probe phase mismatch is considered and another in which the pump-probe phase mismatch is arbitrarily set to zero. These two situations will be referred to as the $\delta k_0 \neq 0$ and $\delta k_0 = 0$ cases, respectively.

In Fig. 2 we show some squeezing-intensity plots with $\Delta_p = 100$ and an infinite L . In curve A $\delta k_0 = 0$, while in curve B the pump-probe phase mismatch δk_0 is taken into account. Both are for the collisionless limit of $F = 1$. Since the short-medium parameter $\beta_c = 100$ for $\Delta_p = 100$, squeezing will exist all the way up to $\beta = 100$ in the short-medium limit. Looking at the regions of squeezing for curves A and B, however, we see that the range of β values for which squeezing occurs is greatly reduced when $L \rightarrow \infty$. Moreover, comparing curve A with B, we find that, although the maximum amount of achievable squeezing is larger for the $\delta k_0 = 0$ case, the range of β values for which squeezing occurs is actually larger for the $\delta k_0 \neq 0$ case.

The reason for the above increase in range is that the stability-rate condition is better satisfied for the $\delta k_0 \neq 0$ case because $\delta k_0 \neq 0$ makes W_{R0} smaller [see Eq. (3.17)]. To confirm this observation, in Fig. 3 we plot μ_{0-}/α_a as a function of β for the two cases being compared. We see that the stability-rate condition is satisfied (i.e., $\mu_{0-} > 0$) only for $\beta < 14$ in the $\delta k_0 = 0$ case (curve A), whereas it is satisfied over the entire range $0 \leq \beta \leq 100$ for the $\delta k_0 \neq 0$ case (curve B). The crossover value of 14 for curve A is as predicted by inequality (6.12). Since, when the stability-rate condition is satisfied, $\delta X^1(\theta_{\min})$ is not necessarily given by Eq. (6.13), the ordinate values for curve A in the $\beta < 14$ region and those for the entire curve B were computed numerically by varying θ iteratively in order to minimize $\delta X^1(\theta)$. In this computation, we made L_c increasingly large to obtain the $L \rightarrow \infty$ limit.

It is interesting to note that for the parameters considered here the relatively lossless and the ideal-noise conditions are satisfied for $14.1 < \beta < 53.2$, which approximately covers the entire region where good squeezing occurs in both the $\delta k_0 = 0$ and $\delta k_0 \neq 0$ cases (see curves A and B in Fig. 2).

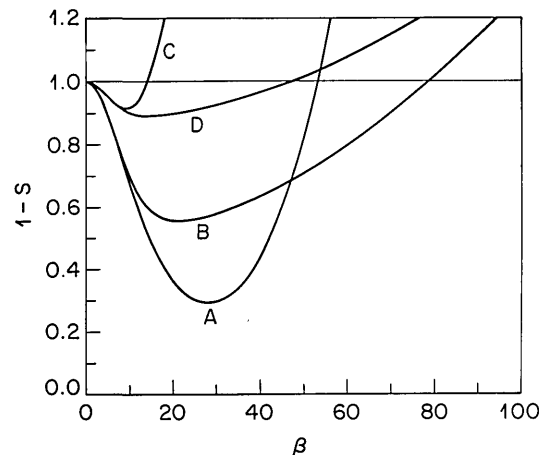


Fig. 2. Squeezing-intensity plots for degenerate infinite-medium case with and without $\delta k_0 = 0$ (curves A versus B) and with and without collisions (curves C versus A and D versus B). Curve A, $\Delta_p = 100$, $\delta k_0 = 0$, and $F = 1$; curve B, $\Delta_p = 100$, $\delta k_0 \neq 0$, and $F = 1$; curve C, same as curve A but with $F = 0.5$; curve D, same as B but with $F = 0.5$.

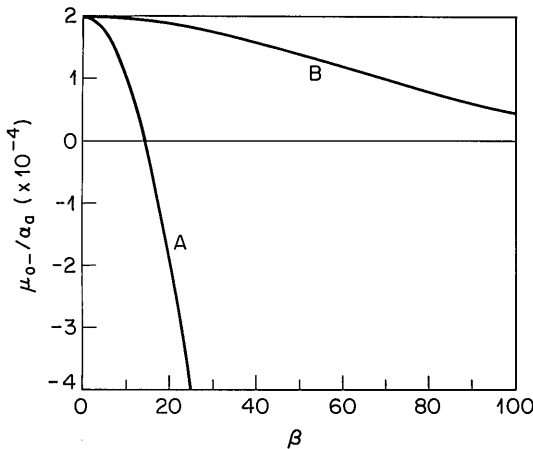


Fig. 3. Stability-rate condition. Curves A and B are for the parameters corresponding to curves A and B, respectively, of Fig. 2.

B. Degenerate Case with Atomic Collisions

What happens when we include atomic collisions, i.e., when the value of F is below unity? Since the dimensionless quantities β^2 , L_a , and Δ_p are proportional to $1/\gamma_{\perp}$, they scale with F . In other words, with collisions, β^2 , L_a , and Δ_p will achieve the same values as those without collisions only if the physical values for the pump intensity, the medium length, and the pump-frequency detuning, respectively, are correspondingly increased. The higher pump intensity and the longer medium required would thus make the occurrence of squeezing more difficult in general. Moreover, the noise correlations depend explicitly on F , even when they are expressed in terms of the normalized parameters. This added dependence on F gives additional effects that are due to collisions.

To see the effect of collisions on squeezing, we varied the value of F and kept the other normalized parameters constant. For example, curves C and D in Fig. 2 are plotted with the same parameters as are curves A and B, respectively, but with $F = 0.5$. Comparing the two sets of curves, we see that the amount and the region of squeezing are drastically reduced as F decreases from 1 to 0.5. Thus atomic collisions can be detrimental to squeezing in the degenerate-frequency limit.^{4,9}

C. Nondegenerate Case

Are there regions where the stability-phase condition can be satisfied at nondegenerate frequencies? Because of the algebraic complexity of the nondegenerate-frequency case, we have resorted to numerical computations to locate such regions. To illustrate the amount of squeezing at nondegenerate frequencies, i.e., to obtain the squeezing spectrum, it is convenient to plot $1 - \mathcal{S}$ as a function of the probe-frequency detuning δ_m . In order to compute \mathcal{S} , we need to know θ_{\min} at each δ_m . There is, in general, no simple analytic formula for θ_{\min} . Instead we obtain the value of $\delta X^1(\theta_{\min})$ by varying θ iteratively to minimize $\delta X^1(\theta)$. Below we shall compare the $\delta k_m = 0$ and the $\delta k_m \neq 0$ cases in order to see the effect of the pump-probe phase mismatch. The effect of collisions will be considered in Section 8.

Figure 4 shows some squeezing spectra obtained with $\Delta_p = 100$, $\beta = 40$, $F = 1$, and an infinite L . Curve A is

with $\delta k_m = 0$, while curve B shows the result with $\delta k_m \neq 0$. The former basically consists of three sharp dips, one at zero frequency, another at a frequency between zero and Δ_R (specifically, $\delta_m = 7.18$), and the third at the generalized Rabi frequency $\Delta_R = 107.7$. The first two dips are really just points of measure zero. The third dip, however, has a finite width of ~ 0.25 as measured at the shot-noise level. For clarity, in the inset we have shown a magnified version of this third dip.

The reason for the first two dips is apparently different from that for the third. Further numerical computation shows that the stability-phase condition is satisfied with equality at the first two dips in curve A. Satisfaction of the stability-phase condition can be tied to Q_m 's becoming purely imaginary at the first dip and zero at the second. As mentioned in Subsection 6.A, when Q_m is zero or purely imaginary the stability-phase condition can be explicitly shown to be satisfied with equality. The stability-rate condition, however, is violated near the first two dips, explaining why these dips are of measure zero. It turns out that, although the stability-phase condition is violated at the third dip, the stability-rate condition is satisfied there. In fact, in curve A the only place where the stability-rate condition is satisfied is a region of approximate width 0.35 near the third dip. This explains why the third dip is of nonzero width. It is interesting to note that the position of the second dip usually increases with increasing β . For example, the second dip shifts to $\delta_m = 25$ for $\beta = 100$. We have also seen the second dip move toward $\delta_m = 0$ and ultimately disappear when β is decreased. The position of the third dip, of course, also shifts with β as the Rabi frequency is β dependent.

In Fig. 4, curve B, which shows the squeezing spectrum with the pump-probe phase mismatch included, is characterized by an unbounded region between $\delta_m = 2.5$ and $\delta_m = 42.5$. Outside this region we obtain a broad region with squeezing. Once again, further numerical computation shows that the stability-phase condition for curve B is violated everywhere except at the zero frequency. We find that with nonzero pump-probe phase mismatch there is no particular probe frequency where Q_m becomes either zero or purely imaginary. This may be the reason for the

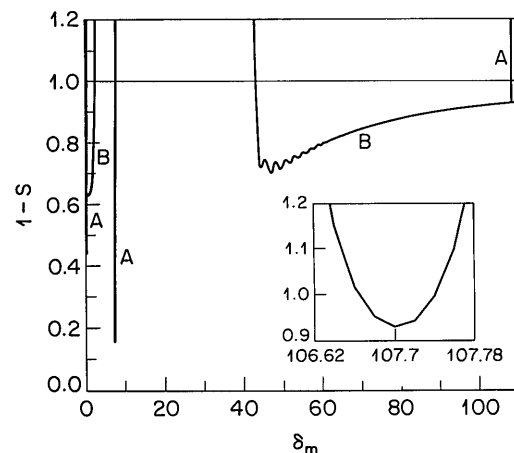


Fig. 4. Squeezing spectra for nondegenerate infinite-medium case, with and without $\delta k_m = 0$ (curve A versus B). For curve A, $\Delta_p = 100$, $\beta = 40$, $\delta k_m = 0$, and $F = 1$; curve B, same as curve A except $\delta k_m \neq 0$; inset, the region around the third dip, i.e., around $\delta_m = 107.7$ of curve A, is enlarged.

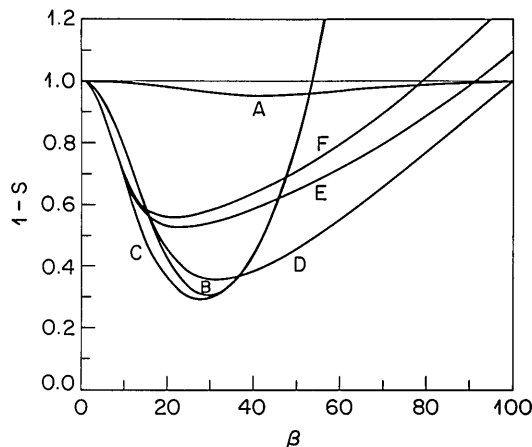


Fig. 5. Squeezing-intensity plots at the degenerate frequency for a finite medium with and without $\delta k_0 = 0$ (curves A, B, and C versus D, E, and F). Curve A, $\Delta_p = 100$, $\delta k_0 = 0$, $F = 1$, and $L_a = 50$; curve B, same as curve A but $L_a = 4000$; curve C, same as curve A but $L_a = \infty$; curve D, $\Delta_p = 100$, $\delta k_0 \neq 0$, $F = 1$, and $L_a = 4000$; curve E, same as curve D but $L_a = 20,000$; curve F, same as curve D but $L_a = \infty$.

impossibility of satisfying the stability-phase condition. Despite the fact that the stability-phase condition is worse in curve B than in curve A, it turns out that the stability-rate condition is better. In fact, the latter is violated only within the unbounded region of curve B. This explains why in curve B there is a broad range of δ_m values where squeezing exists. Furthermore, the reason for the better stability-rate condition for curve B is the same as that quoted for the $\delta k_m \neq 0$ case in Subsection 6.A.

7. SQUEEZING IN A LONG MEDIUM: DEGENERATE CASE

In this section we consider squeezing at the degenerate frequency in a long but finite medium of length L_a . We shall not discuss the effect of collisions, which was treated in Section 6. Instead we shall consider the effects of Doppler broadening in the atomic medium and Gaussian-intensity variation of the pump beam.

A. Simple Degenerate Case

We first explore the simplest case, in which the effects of collisions, Doppler broadening, and Gaussian-intensity variation are ignored. Figure 5 shows some squeezing-intensity plots for different values of L_a with $\Delta_p = 100$ and $F = 1$. These plots with different L_a values enable us to see how the transition from a short to a long medium takes place.

Curves A, B, and C are plotted in Fig. 5 with $\delta k_0 = 0$ and L_a set equal to $0.005\Delta_p^2$, $0.4\Delta_p^2$, and ∞ , respectively. We see that the squeezing curves quickly approach the infinite-medium curve C as L_a becomes large compared with Δ_p^2 . Such behavior is expected, since Eqs. (3.15) and (6.7) tell us that when $L_a > \Delta_p^2$ (with $|\Delta_p| > 1$ and $\beta^2 < 2\Delta_p^2$), $S_{R0}L$ becomes large compared with unity, causing U_{m+} , U_{m-} , A_{m+} , and A_{m-} to approach their infinite-medium values.

In curves D, E, and F of Fig. 5 we include the effect of pump-probe phase mismatch, i.e., $\delta k_0 \neq 0$ and L_a is set equal to $0.4\Delta_p^2$, $2\Delta_p^2$, and ∞ , respectively. $L_a = 0.4\Delta_p^2$

happens to give the maximum amount of squeezing, which is not obtained with an infinite L_a , as is the case when $\delta k_0 = 0$. Thus we find that *with the pump-probe phase mismatch included, there is an L_a value that optimizes the maximum amount of squeezing.* Below, we shall refer to such L_a value as L_{opt} . Moreover, comparing curve D with C, we see that the maximum amount of squeezing achievable with the inclusion of the pump-probe phase mismatch is only slightly less than that for the case when it is ignored.

We further note that curve A of Fig. 5 really illustrates the case of a short medium, showing squeezing all the way up to $\beta = \beta_c = 100$, with β_c as defined below inequality (5.10). In this short-medium limit the squeezing-intensity curve is insensitive to inclusion of the pump-probe phase mismatch. Also, when L_a is optimally chosen with $\delta k_0 \neq 0$ (curve D), squeezing occurs all the way up to $\beta = 100$, which is, surprisingly, as wide as the region of squeezing in the short-medium limit.

B. Dependence on Pump Detuning

To see how the maximum amount of achievable squeezing increases with the pump-frequency detuning, we show some squeezing-intensity plots for different values of Δ_p . Curves A, B, C, and D of Fig. 6 are plotted with $F = 1$, $\delta k_0 = 0$, and $L_a = \infty$ and the pump detuning Δ_p set equal to 0, 10, 100, 1000, respectively. We find that in order to achieve more than 70% squeezing at the degenerate frequency, one must have Δ_p larger than 100.

C. Effect of Doppler Broadening

Doppler broadening exists if one uses an atomic vapor instead of an atomic beam as the interaction medium. Its effect can be included by integrating \tilde{X}_0 , $\tilde{\gamma}_0$, Λ_0 , and R_0 over different resonance frequencies of the moving atoms. The procedure for doing the integrations is detailed in Appendix A. The normalized Doppler half-width, defined in Appendix A, will be denoted by Δ_{dhw} . It is related to the Doppler FWHM Δ_{FWHM} by $\Delta_{dhw} \approx 0.6\Delta_{FWHM}$. The pump detuning Δ_p is to be replaced by Δ_{ps} , which describes the normalized detuning of the pump frequency from the center of the Doppler-frequency distribution.

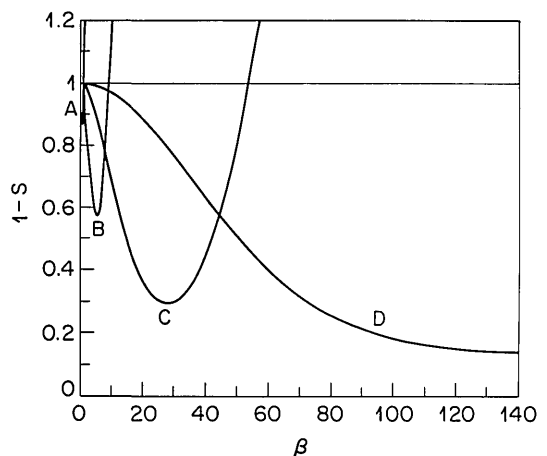


Fig. 6. Squeezing-intensity plots at the degenerate frequency for a finite medium with different values of Δ_p . Curve A, $\Delta_p = 0$, $\delta k_0 = 0$, $F = 1$, and $L_a = \infty$; curve B, same as curve A but $\Delta_p = 10$; curve C, same as curve A but $\Delta_p = 100$; curve D, same as curve A but $\Delta_p = 1000$.

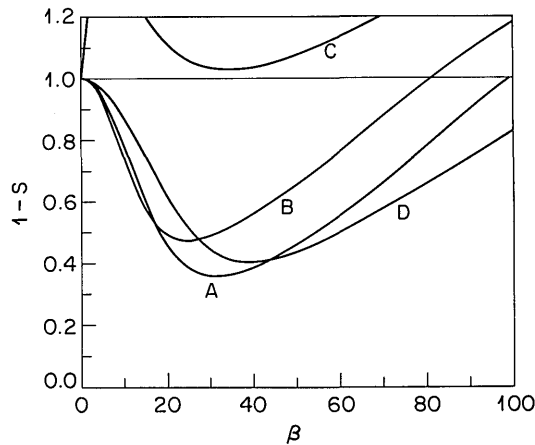


Fig. 7. Squeezing-intensity plots at the degenerate frequency for a finite medium with varied Doppler width (curves A, B, and C). The effect of Gaussian-intensity variation is illustrated by curve D, which should be compared with curve A (the uniform-intensity case). Curve A, $\Delta_{ps} = 100$, $\delta k_0 = 0$, $F = 1$, $L_a = 4000$, and $\Delta_{dhw} = 0$; curve B, same as curve A but $\Delta_{dhw} = 0.33\Delta_p$; curve C, same as curve A but $\Delta_{dhw} = 0.50\Delta_p$; curve D, same as curve A but with the Gaussian-intensity variation included so that the horizontal axis should be interpreted as β_{pk} .

Figure 7 shows some squeezing-intensity plots with $\Delta_{ps} = 100$, $L_a = 4000 = 0.4\Delta_{ps}^2$, $F = 1$, and the pump-probe phase mismatch included. Curves A, B, and C are plotted with the Doppler widths Δ_{dhw} set equal to 0, $0.33|\Delta_{ps}|$, and $0.5|\Delta_{ps}|$, respectively. We see that curve B is close to the Doppler-free case illustrated by curve A. In other words, the effect of Doppler broadening becomes negligible when the pump is detuned by more than three Doppler half-widths, i.e., $|\Delta_{ps}| > 3\Delta_{dhw}$.

D. Effect of Gaussian-Intensity Variation

Gaussian-intensity variation of the laser beam gives rise to a nonuniform excitation of the atoms across the pump beam. As discussed in Appendix B, the effect of Gaussian-intensity variation can be taken into account similarly to the effect of Doppler broadening by integrating the various coefficients and noise correlations over the variation in the pump-beam intensity seen by the different atoms. In this treatment the probe beams are assumed to have the same Gaussian intensity profile as the pump beam. When the Gaussian-intensity variation is included, the parameter β is replaced by β_{pk} which is defined in terms of the peak intensity of the Gaussian-intensity profile (see Appendix B). Furthermore, in this paper we assume that δk_m^s does not depend upon the transverse position across the beam. As is explained in Appendix B, this amounts to neglecting the effect of self focusing or defocusing, a preliminary account of which is presented in Section 9.

As an illustration of the effect of Gaussian-intensity variation, curve D of Fig. 7 is plotted with the same parameters as curve A but with the Gaussian-intensity variation included. The horizontal axis of curve D is to be taken as β_{pk} . Comparing curve D with the uniform-intensity case depicted by curve A, we see that in the ideal-noise region where β_{pk} is small the amount of squeezing for curve D at a particular β_{pk} value is the same as that for curve A at $\beta \approx 0.7\beta_{pk}$. One can thus take the effective intensity of the Gaussian beam to be approximately 0.5 times its peak value and estimate the amount of

squeezing from the uniform-intensity case. However, in the region where β_{pk} is large (violating the ideal-noise condition $|\Delta_p|^3 > \beta_{pk}^4/8$), so that the effect of spontaneous emission dominates, such a simple effective-intensity formula does not succeed. This is because when β_{pk} is large the atoms that see a higher intensity may actually generate less squeezing than those that see a lower intensity.

8. SQUEEZING IN A LONG MEDIUM: NONDEGENERATE CASE

In this section we consider squeezing at nondegenerate frequencies in a long but finite medium of length L_a . We shall comprehensively discuss the effects of collisions, pump-probe phase mismatch, Doppler broadening in the atomic medium, and Gaussian-intensity variation of the pump beam.

A. Simple Nondegenerate Case

We start by exploring the simplest case, in which the effects of pump-probe phase mismatch, collisions, Doppler broadening, and Gaussian-intensity variation are neglected. Figure 8 shows some squeezing spectra for different values of L_a with $\Delta_p = 100$, $F = 1$, and $\beta = 40$. Plots of this kind with different values of L_a allow us to see how the transition from a short to a long medium takes place.

Curves A, B, C, D, and E are plotted with L_a equal to $0.0001\Delta_p^2$, $0.001\Delta_p^2$, $0.01\Delta_p^2$, $0.3\Delta_p^2$, and $0.6\Delta_p^2$, respectively. The $L_a = 0.0001\Delta_p^2$ case describes the squeezing spectrum of a short medium; it agrees with the squeezing spectrum of resonance fluorescence given in Ref. 10. The short-medium squeezing spectrum is characterized by a single dip at the generalized Rabi frequency Δ_R . As L_a increases, the amount of squeezing at the generalized Rabi frequency stays at the same value while the amounts between $\delta_m = 0$ and $\delta_m = \Delta_R$ fall below it. When $L_a > 0.3\Delta_p^2$, the squeezing spectrum begins to approach that for an infinitely long medium characterized by three dips. The formation of these three dips is already apparent in

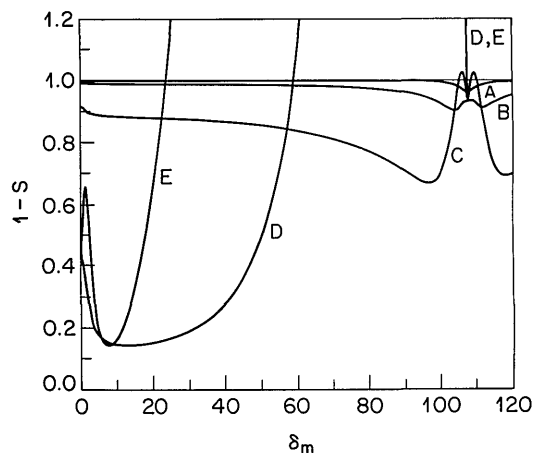


Fig. 8. Squeezing spectra for a finite medium of various lengths L_a when the effects of collisions, pump-probe phase mismatch, Doppler broadening, and Gaussian-intensity variation are ignored. Curve A, $\Delta_p = 100$, $\beta = 40$, $\delta k_m = 0$, $F = 1$, and $L_a = 1$; curve B, same as curve A but $L_a = 10$; curve C, same as curve A but $L_a = 100$; curve D, same as curve A but $L_a = 3000$; curve E, same as curve A but $L_a = 6000$.

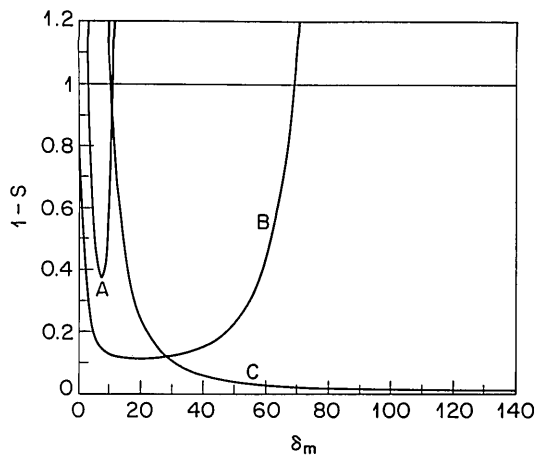


Fig. 9. Squeezing spectra for a finite medium with different values of Δ_p when the effects of collisions, pump-probe phase mismatch, Doppler broadening, and Gaussian-intensity variation are ignored. Curve A, $\Delta_p = 10$, $\beta = 15$, $L_a = 100$, $\delta k_m = 0$, and $F = 1$; curve B, same as curve A but $\Delta_p = 100$, $\beta = 50$, and $L_a = 2000$; curve C, same as curve A but $\Delta_p = 1000$, $\beta = 500$, and $L_a = 50,000$.

curve E. The maximum amount of squeezing in curve E is achieved at the second dip and the value is quite close to that for an infinitely long medium.

B. Dependence on Pump Detuning

To illustrate how the amount of squeezing at nondegenerate frequencies increases with the pump-frequency detuning, in Fig. 9 we show some squeezing spectra for different values of Δ_p with $F = 1$ and $\delta k_m = 0$. Curves A, B, and C are plotted with $\Delta_p = 10$, $\beta = 15$, $L_a = 100$, $\Delta_p = 100$, $\beta = 50$, $L_a = 2000$, and $\Delta_p = 1000$, $\beta = 500$, $L_a = 50,000$, respectively. The value of L_a in each case is chosen to obtain a broadband region of large squeezing. The maximum amount of squeezing would increase further with β ; we picked a particular value in each case just for the purpose of illustration. It is clear that greater than 60% squeezing can be obtained with $\Delta_p > 10$. As compared with squeezing at the degenerate frequency (Figs. 5 and 6), we see that at nondegenerate frequencies the same maximum squeezing can be achieved with a smaller pump-frequency detuning.

C. Effect of Pump-Probe Phase Mismatch

What happens when we take into account the pump-probe phase mismatch? To demonstrate the effect, in Fig. 10 we show some squeezing spectra with the same Δ_p , F , and β values as those in Fig. 8 but including pump-probe phase mismatch in their calculation. In Fig. 10 curves A, B, C, and D are plotted with L_a set equal to $0.0001\Delta_p^2$, $0.01\Delta_p^2$, $0.3\Delta_p^2$, and Δ_p^2 , respectively. Comparing curve B of Fig. 10 with curve C of Fig. 8, we see that the inclusion of pump-probe phase mismatch leads to a series of wiggles in the squeezing spectra near the generalized Rabi frequency. In fact, further numerical computation shows that the wiggle period corresponds to a change in the value of $\delta k_m^s L$ by 2π . The wiggles appear near the generalized Rabi frequency because there the value of $\delta k_m^s L$ changes extremely rapidly.

Parameters for curve C in Fig. 10 happen to give approximately the maximum amount of squeezing. Again,

we find that the maximum is obtained at a finite medium length when $\delta k_m \neq 0$. Furthermore, comparing curve C of Fig. 10 with curve E of Fig. 8, we see that the maximum amount of squeezing achievable with $\delta k_m \neq 0$ is not greatly different from that with $\delta k_m = 0$. Curve C of Fig. 10 also shows that the range of δ_m values for which squeezing occurs can be larger with $\delta k_m \neq 0$ than with $\delta k_m = 0$. The reason for this larger range is the same as that discussed in Subsection 6.C.

D. Effect of Increased Pump Intensity

What happens as we change the pump intensity? To illustrate the effect, Fig. 11 shows squeezing spectra for different values of β with $\Delta_p = 100$, $F = 1$, and $\delta k_m \neq 0$. Curves A, B, and C are plotted with $\beta = 0.4\Delta_p$, Δ_p , and $2\Delta_p$, respectively, and $L_a = 3000$, which approximately maximizes the amount of squeezing in each case (i.e., $L_a = L_{\text{opt}}$ with L_{opt} as defined in Subsection 7.A). We find that as β becomes larger than Δ_p the region of squeezing suddenly broadens. This broadening is apparently due to a sudden shift in the generalized Rabi frequency to a higher value, as the pump intensity crosses the (detuned) saturation threshold. Thus, unlike at the degenerate frequency, squeezing at nondegenerate frequencies can actually be better with a pump intensity that is larger than the saturation intensity for the atomic medium (but see Subsections 8.F and 8.G below).

Besides the broadening, the minimum δ_m at which squeezing occurs also increases with the pump intensity. Such behavior is consistent with the prediction of δ_c with δ_c as defined after Eq. (5.17). For example, we see that squeezing begins at $\delta_m = 3.5$ in curve C, while δ_c for the parameters of curve C is approximately 4 [estimated by using Eq. (5.17)].

One may also wonder what the squeezing-intensity curve is like at a nondegenerate frequency, i.e., at $\delta_m \neq 0$. Curve A in Fig. 12 shows a squeezing-intensity plot at $\delta_m = 20$, $\Delta_p = 100$, $F = 1$, $L_a = 3000$, and $\delta k_m \neq 0$. We see that the region of squeezing goes from $\beta = 0$ all the way up to $\beta = 1000$. The upper value of $\beta = 1000$ can be predicted by using Eq. (5.17) [or when $\delta_m \ll 1$, by using Eq. (5.15)], taking δ_c to be δ_m and solving for β . In fact,

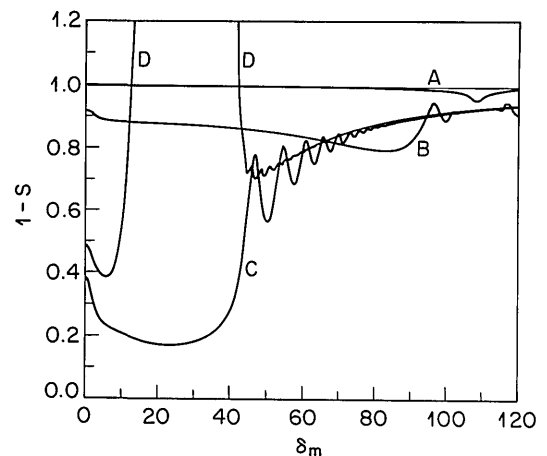


Fig. 10. Squeezing spectra for a finite medium of length L_a with the effect of pump-probe phase mismatch included (contrast with Fig. 8). Curve A, $\Delta_p = 100$, $\beta = 40$, $\delta k_m \neq 0$, $F = 1$, and $L_a = 1$; curve B, same as curve A but $L_a = 100$; curve C, same as curve A but $L_a = 3000$; curve D, same as curve A but $L_a = 10,000$.

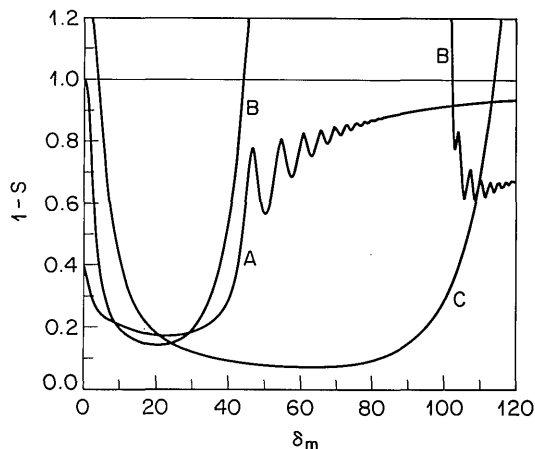


Fig. 11. Squeezing spectra for a finite medium with various values of β . Curve A, $\Delta_p = 100$, $\beta = 40$, $\delta k_m \neq 0$, $F = 1$, and $L_a = 3000$; curve B, same as curve A but $\beta = 100$; curve C, same as curve A but $\beta = 200$.

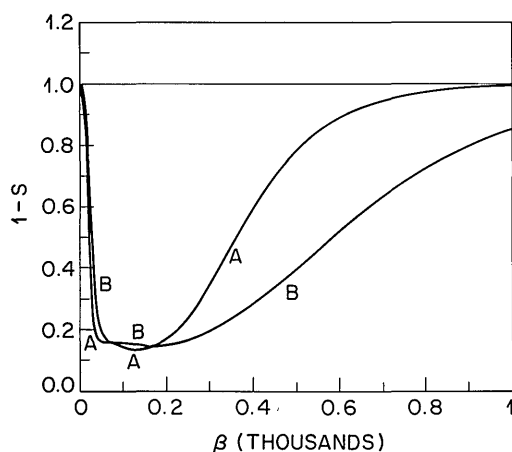


Fig. 12. Squeezing-intensity plot for a medium of finite length at a nondegenerate frequency. Curve A, $\delta_m = 20$, $\Delta_p = 100$, $F = 1$, $L_a = 3000$, $\delta k_m \neq 0$, and $\Delta_{dhw} = 0$; curve B, same as curve A but with the inclusion of Gaussian-intensity variation of the pump beam (the horizontal axis should be interpreted as β_{pk}).

applying Eq. (5.17) to the case illustrated by curve A in Fig. 12 (i.e., by letting $\delta_c = 20$), we obtain $\beta = 1000$ as the exact upper cutoff.

E. Effect of Collisions

As mentioned in Section 6, when there are collisions the dimensionless quantities β^2 , L_a , Δ_p , and δ_m are scaled with the collision factor F . As a result, the same values of β^2 , L_a , Δ_p , and δ_m can be achieved by only physically increasing the pump intensity, the medium length, the pump-frequency detuning, and the probe-frequency detuning, respectively, thus making it harder to achieve squeezing.

To show the additional effects that are due to collisions, we shall change the value for F while keeping the other parameters fixed. Curves A and B of Fig. 13 are squeezing spectra for $F = 1$ and $F = 0.5$, respectively, with $\beta = 40$, $\Delta_p = 100$, $\delta k_m \neq 0$, and $L_a = 3000 = L_{opt}$. We see that, although there is a drastic decrease in the amount of squeezing near the degenerate frequency, the change is much less serious at nondegenerate frequencies that are only a few linewidths away.⁹

Curves C, D, and E of Fig. 13 depict other examples, which are squeezing spectra for $F = 1$, $F = 0.2$, and $F = 0.02$, respectively, with $\Delta_p = 100$, $\beta = 200$, and $L_a = 800$. These curves illustrate the above-saturation case when $\beta > |\Delta_p|$. Because $\Omega_R^2 = \beta^2 F + \Delta_p^2$, there is a pronounced shift in the generalized Rabi frequency caused by collisions. In order to show more clearly the associated shift in the noise structure that is a signature of the region around the generalized Rabi frequency, we chose $L_a < L_{opt}$ in this example.

When collisional broadening is large (i.e., $F \ll 1$), there is an enhanced structure in the squeezing spectrum near the zero frequency that can be attributed to coherent population oscillations. To show this additional structure, we have plotted curve F in Fig. 13, which is the same as curve E but magnified 50 times horizontally and 5 times vertically. The hump near the zero frequency is clearly visible. Similar humps in the loss coefficient and the coupling coefficient are responsible for the observed hump in the squeezing spectrum.⁵

F. Effect of Doppler Broadening

To study the effect of Doppler broadening, in Fig. 14 we show some squeezing spectra with $\Delta_{ps} = 100$, $\beta = 40$, $F = 1$, and $\delta k_m \neq 0$. Curves A, B, and C are for Δ_{dhw} set equal to $0.33\Delta_{ps}$, $0.5\Delta_{ps}$ and $2\Delta_{ps}$, respectively, and $L_a = 3000 = L_{opt}$. These are to be compared with curve D of Fig. 8, which shows a squeezing spectrum with the same parameters but without Doppler broadening. It is evident that the effect of Doppler broadening becomes negligible only when Δ_{ps} is detuned by more than $3\Delta_{dhw}$, which agrees with the observation made in Subsection 7.C. Moreover, we see that when $\Delta_{dhw} > 0.5\Delta_{ps}$ (curves B and C), there are some noise peaks in the squeezing spectra near $\delta_m = 40 = \beta$. These noise peaks come from those usually appearing near the generalized Rabi frequency. In this case the generalized Rabi frequency is equal to β because, effectively, most of the atoms have $\Delta_p = 0$ when the pump detuning is within a Doppler half-width. Thus the location of these peaks is expected to shift if we vary

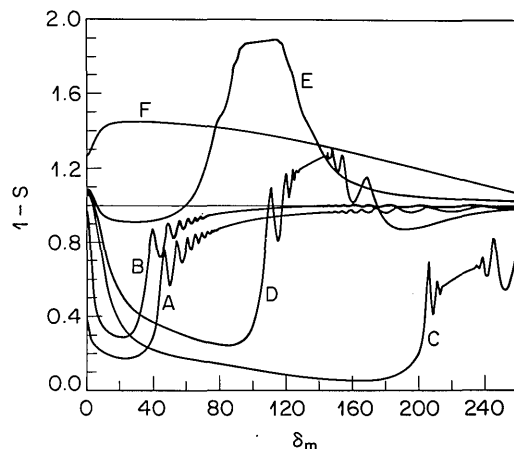


Fig. 13. Effect of collisions on squeezing spectra for a medium of finite length. Curve A, $\Delta_p = 100$, $\beta = 40$, $\delta k_m \neq 0$, $F = 1$, and $L_a = 3000$; curve B, same as curve A but $F = 0.5$; curve C, $\Delta_p = 100$, $\beta = 200$, $\delta k_m \neq 0$, $F = 1$, and $L_a = 800$; curve D, same as curve C but $F = 0.2$; curve E, same as curve C but $F = 0.02$; curve F, same as curve E but magnified 50 times horizontally and 5 times vertically.

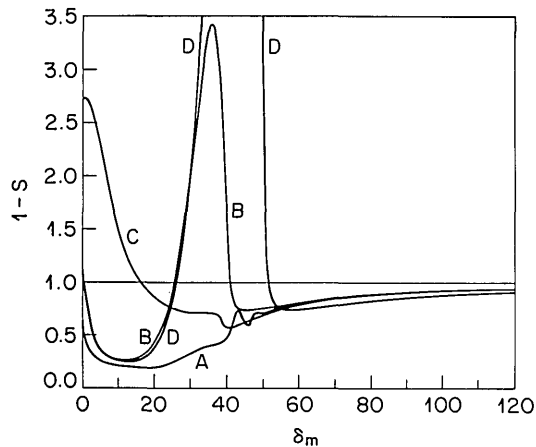


Fig. 14. Effect of Doppler broadening on squeezing spectra for a medium of finite length with different values of Δ_{dhw} and β . Curve A, $\Delta_{ps} = 100$, $\Delta_{\text{dhw}} = 33$, $\beta = 40$, $\delta k_m \neq 0$, $F = 1$, and $L_a = 3000$; curve B, same as curve A but $\Delta_{\text{dhw}} = 50$; curve C, same as curve A but $\Delta_{\text{dhw}} = 200$; curve D, same as curve B but $\beta = 50$.

the value of β . For example, in curve D of Fig. 14 we have increased β to 50 while keeping the other parameters the same as in curve B; the edge of the peak has clearly shifted to $\delta_m = 50$.

One may ask, What determines the residual structure in the squeezing spectrum of curve C when $|\Delta_{ps}| < \Delta_{\text{dhw}}$? The squeezing spectrum in this limit is basically an average of several Doppler-free squeezing spectra, with Δ_p taken within the Doppler width and L_a set to a reduced value. It is interesting to note that the remaining structure may, therefore, be quite different from that in the Doppler-free squeezing spectrum with zero detuning ($\Delta_p = 0$).

G. Effect of Gaussian-Intensity Variation

To study the effect of Gaussian-intensity variation and to compare it with the uniform-intensity case, in Fig. 12 we showed a squeezing-intensity plot at the nondegenerate frequency of $\delta_m = 20$. Curve A is the uniform-intensity case with $\Delta_p = 100$, $\Delta_{\text{dhw}} = 0$, $F = 1$, $L_a = 3000$, and $\delta k_m \neq 0$. Curve B is plotted with the same parameters as curve A but with the Gaussian-intensity variation of the pump beam considered, so that the horizontal axis is to be interpreted as β_{pk} . Just as at the degenerate frequency (compare Fig. 7), we see that for small β values the Gaussian-intensity case can be well approximated by the uniform-intensity case, provided that in the latter the pump intensity is taken to be half the peak intensity of the Gaussian beam in the former. Again, for large β values such a simple formula breaks down for the same reason discussed in Subsection 7.D.

What happens when we have Gaussian-intensity variation of the pump beam in addition to Doppler broadening in the atomic medium? In Subsection 8.F we saw that, when $|\Delta_p|$ is less than twice the Doppler half-width Δ_{dhw} , the location of the peaks in the squeezing spectrum shifts with the pump intensity. Thus we would expect the squeezing spectrum to change dramatically if the pump beam has Gaussian-intensity variation. This situation is shown in curve A of Fig. 15, where a squeezing spectrum is plotted with the same parameters as curve B

of Fig. 14 except that we have included the effect of Gaussian-intensity variation by setting $\beta_{pk} = 40$. We see that there is a series of peaks in the region where squeezing would have been obtained were it not for the Gaussian pump intensity. The combination of Doppler broadening and Gaussian-intensity variation, therefore, can catastrophically alter the squeezing spectrum. This problem can be remedied, however, by tuning the pump frequency further than three Δ_{dhw} . This is shown in curve B of Fig. 15, which is plotted with the same parameters as curve A but with $\Delta_{\text{dhw}} = 0.33\Delta_{ps}$.

Even if the pump frequency is detuned far outside the region where Doppler broadening is important, the location of the generalized Rabi frequency is still sensitive to the pump intensity. One may thus wonder what effect Gaussian intensity has on the noise structure near the generalized Rabi frequency. In order to illustrate the effect, in Fig. 16 we show some squeezing spectra for different values of β and L_a with $\Delta_{\text{dhw}} = 0$, $\delta k_m \neq 0$, and $\Delta_{ps} = 100$. Curves A, B, and C are with $\beta = 40$, $L_a = 3000$, $\beta = 100$, $L_a = 100$, and $\beta = 200$, $L_a = 800$, respectively. Comparing these with the uniform-intensity curves with the same parameters (curves A and C of Fig. 13), we see that the Gaussian-intensity variation can give rise to a series of peaks between the highest generalized Rabi frequency $\Omega_R = (\Delta_p^2 + \beta^2)^{1/2}$ and the lowest generalized Rabi frequency $\Omega_R = |\Delta_p|$ experienced by the atoms. The peaks are especially pronounced in the above-saturation case (curve C), which would exhibit good squeezing over a wide range of δ_m values were it not for the Gaussian-intensity variation.

9. EFFECT OF SELF-FOCUSING AND DEFOCUSING

The initially Gaussian pump beam propagating through the medium experiences a spatially varying nonlinear refractive index that can cause it to self-focus or defocus. The probe beams also see spatially varying nonlinear refractive indices, which, moreover, are different from the one seen by the pump beam. In our atomic-vapor experiments that generated squeezed light,³ self-focusing or de-

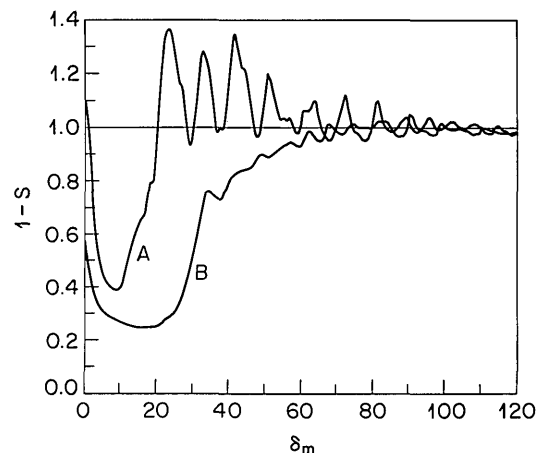


Fig. 15. Effect of Gaussian-intensity variation and Doppler broadening on squeezing spectra for a finite medium. Curve A, $\Delta_{ps} = 100$, $\Delta_{\text{dhw}} = 50$, $\beta_{pk} = 40$, $\delta k_m \neq 0$, $F = 1$, and $L_a = 3000$; curve B, same as curve A but $\Delta_{\text{dhw}} = 33$.

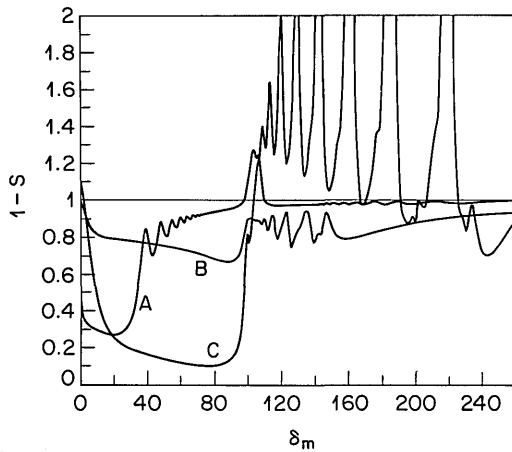


Fig. 16. Effect of Gaussian-intensity variation on squeezing spectra for a finite medium. Curve A, $\Delta_{ps} = 100$, $\Delta_{dhw} = 0$, $\delta k_m \neq 0$, $F = 1$, $\beta_{pk} = 40$, and $L_a = 3000$; curve B, same as curve A but $\beta_{pk} = 100$ and $L_a = 100$; curve C, same as curve A but $\beta_{pk} = 200$ and $L_a = 800$.

focusing was a readily observed and pronounced effect. This self-focusing or defocusing of the pump and probe beams is a serious problem in the achievement of squeezing and will be the subject of this section.

A. Degenerate Case

First we examine the self-focusing or defocusing behavior of the pump and probe beams when their frequencies are the same. Simple expressions for the pump-intensity-dependent phase shifts can be obtained. When the pump intensity is below saturation, the intensity-dependent part of the pump phase shift $\delta\phi_p$ is approximately given by

$$\delta\phi_p = \frac{\alpha_a L \beta^2}{2\Delta_p^3}. \quad (9.1)$$

Note that the pump phase shift is only $\tilde{\gamma}_p L$ [compare Eqs. (2.32) and (2.33)] when the refractive index n_p is close to unity. Assuming that $|\Delta_p| \gg 1$, using Eq. (2.10), and expanding the denominator of $\tilde{\gamma}_p$ to first order, we easily obtain the above expression for $\delta\phi_p$. Equation (9.1) tells us that, if the pump beam has Gaussian-intensity variation, then the center of the beam experiences a phase shift that is different from that experienced by the wings of the beam profile, thus causing the beam to focus or defocus. Also, from the above expression it is clear that self-focusing will occur when the pump frequency is blue detuned from resonance (i.e., $\Delta_p > 0$) and self-defocusing will occur when the pump frequency is red detuned.

The probe beams, on the other hand, experience a pump-intensity-dependent phase shift

$$\delta\phi_0 = \frac{\alpha_a L \beta^2}{\Delta_p^3}, \quad (9.2)$$

which is obtained by using Eq. (2.10) and expanding the imaginary part of $\tilde{\gamma}_0$ of Eq. (6.7) to first order in $(\beta/\Delta_p)^2$. Thus we see that the pump and probe beams do not experience the same amount of spatially varying intensity-dependent phase shift.

The different amount of focusing or defocusing experienced by the pump and the probe beams implies that our

assuming that the pump and the probe beams share a common spatial-mode profile is not valid, particularly when the focusing or defocusing effect becomes significant. As a first approximation, we assume that there is a probe beam-PCB mode combination that becomes maximally squeezed, with the remaining spatially orthogonal modes experiencing little squeezing. Because of the different amount of focusing or defocusing experienced by the pump and the probe beams, the spatial profile of the maximally squeezed probe beam-PCB mode at the output of the medium will be different from that of the transmitted pump. Experimentally this means that we would not know what spatial profile to use for the LO in order to detect squeezing in the maximally squeezed probe beam-PCB mode. Nevertheless, we would expect that the maximally squeezed probe beam-PCB mode will have an output spatial profile that is somewhat close to that of the transmitted pump beam. Thus one may want to use the transmitted pump as the LO.

We have thus raised two issues here: The first is the breakdown of the simple theoretical model, which assumes a common spatial profile for the pump and the probe beams when they undergo self-focusing or defocusing in the medium; the second is our inability to know the maximally squeezed probe beam-PCB mode at the output of the medium. Although we may not know the maximally squeezed mode, it is still possible to calculate the amount of squeezing in the mode that is detected by the LO by using some numerical methods to account for the effect of self-focusing or defocusing.

Denoting the mismatch $\delta\phi_0 - \delta\phi_p$ by $\delta\phi_{op}$, we see from Eqs. (9.1) and (9.2) that $\delta\phi_{op} = \delta\phi_p$. The mismatch $\delta\phi_{op}$ may not be serious if it occurs in a region where maximum squeezing is already achieved. Unfortunately, such is not the case in a two-level system. To see this, we look at the coupling coefficient \tilde{X}_0 , which is responsible for squeezing in the ideal-noise limit. At the degenerate frequency, from Eq. (6.8), \tilde{X}_0 is given by

$$\tilde{X}_0 = \frac{i\alpha_a \beta^2}{2\Delta_p^3}, \quad (9.3)$$

where we have assumed operation below saturation and $\Delta_p \gg 1$. Clearly $|\tilde{X}_0|L$ is identical to $|\delta\phi_{op}|$. The short-medium squeezing formula tells us that, in order to achieve large squeezing in the ideal limit where $\Lambda_0 = 0$ and $R_0 = |\tilde{X}_0|$, one must have $|\tilde{X}_0|L$ of the order of unity. But then $\delta\phi_{op}$ will also be of the order of unity, indicating potential trouble. Interestingly, it turns out that the above-saturation case also has the same ratio between $\delta\phi_p$ and $\delta\phi_0$, and $|\tilde{X}_0|L = |\delta\phi_{op}|$.

To be more precise, it is necessary to see at what value of $\delta\phi_{op}$ the intensity-dependent phase shift poses a serious problem. Imagine that the pump- and the probe-beam radii are the same but that the wave fronts are phase shifted with respect to each other because of the different refractive indices experienced by these beams. Also, we assume that the phases of the pump and the probe beams are matched in the high-intensity region of the beams and mismatched elsewhere. We call this optimistic assumption minimal mode mismatch. The amount of mode matching M can then be calculated by the usual technique. For the described situation, it is not hard to show that

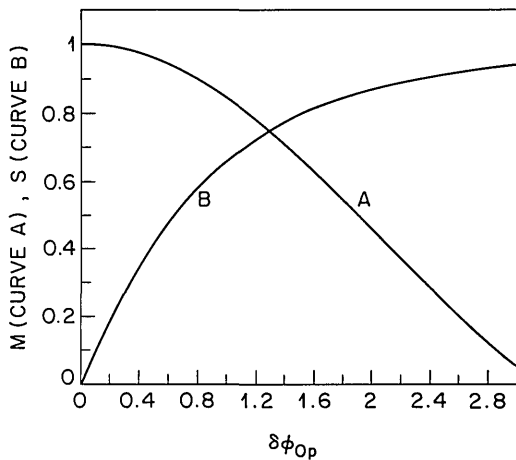


Fig. 17. Pump-probe mode mismatch M (curve A) and amount of squeezing S (curve B) in the ideal lossless limit as a function of $\delta\phi_{op}$.

$$M = \int_0^\infty dr 2\pi r \left(\frac{\exp(-2r^2)}{\pi/2} \right) \cos[\phi(r) - \phi(0)], \quad (9.4)$$

where

$$\phi(r) = \phi(0)\exp(-2r^2), \quad (9.5)$$

and

$$\phi(0) = \delta\phi_{op}, \quad (9.6)$$

with β^2 in $\delta\phi_{op}$ replaced by β_{pk}^2 [the r dependence has been removed in Eq. (9.5)]. We expect the mode mismatch to become significant when, let us say, $M = 0.5$. Thus we want to know the value of $\delta\phi_{op}$ in Eq. (9.4) that yields $M = 0.5$. One can solve for $\delta\phi_{op}$ graphically by plotting M as a function of $\delta\phi_{op}$. This is illustrated by curve A in Fig. 17. We see that at $M = 0.5$, $\delta\phi_{op} = 1.9$. Together with M , it is also interesting to plot the amount of squeezing \mathcal{S} at the degenerate frequency for the ideal lossless case, which we illustrate by curve B in Fig. 17. It is clear that a maximum squeezing of 0.75 occurs with $M = 0.75$. Furthermore, M decreases rapidly with increasing $\delta\phi_{op}$, thus prompting us to conclude that a squeezing of 0.75 is the best that one can hope for. This, of course, is only a rough estimate. To obtain a more accurate estimate, one must numerically integrate the equation of motion for $\alpha_m(Z)$ over the medium length, as is discussed in Appendix B. Our initial numerical results indicate good agreement with the rough estimate, giving a maximum squeezing of about 80%. These further results will be presented elsewhere.

B. Nondegenerate Case

We have discussed above the mode mismatch problem at the degenerate frequency. The discussion is also usually valid at nearly degenerate frequencies when $0 < \delta_m \ll |\Delta_p|$. However, at large δ_m the nonlinear phase shifts for the probe beam and the PCB, denoted by $\delta\phi_m$ and $\delta\phi_{\bar{m}}$, respectively, can have values quite different from each other and from $\delta\phi_p$. As an illustration, we compute $\delta\phi_m$, $\delta\phi_{\bar{m}}$, and $\delta\phi_p$ numerically for the case where $\Delta_p = 100$, $\beta = 40$, $F = 1$, $\Delta_{dhw} = 0$, $\delta k_m \neq 0$, and $L_a = 3000$ and plot them in Fig. 18 as curves A, B, and C, respectively. We

see that the values of $\delta\phi_m$ and $\delta\phi_{\bar{m}}$ are drastically different from each other when the frequency of one of the probe beams (the one with detuning δ_m in this case) passes through the atomic resonance. The values get closer to each other again when $\delta_m > \Delta_R$.

C. Optimum Medium Length

Besides the above-mentioned problem of mode mismatch between the pump and the probe beams, the self-focusing or defocusing of the pump can itself be a problem, as it changes the effective pump intensity within the medium. However, this problem can always be circumvented by a careful choice of the medium length and the pump-beam waist. As we show below, this is possible because the maximum squeezing almost always occurs when $\delta\phi_p \approx \pi$.

Let us estimate the radius of curvature R_b that is acquired by an input beam with a plane wave front as it propagates through the medium. We are particularly interested in the value of R_b when operating near the region of maximum squeezing. We further assume that the input beam does not experience much diffraction in the medium when the medium is inactive. Then when the medium is active, given that the phase front at the beam center is shifted by a small distance Δ_L with respect to the phase front at the beam waist, it is not hard to estimate the radius of curvature acquired by the transmitted beam. In fact, we can make a good estimate by using the simple geometrical picture shown in Fig. 19, where W_b is

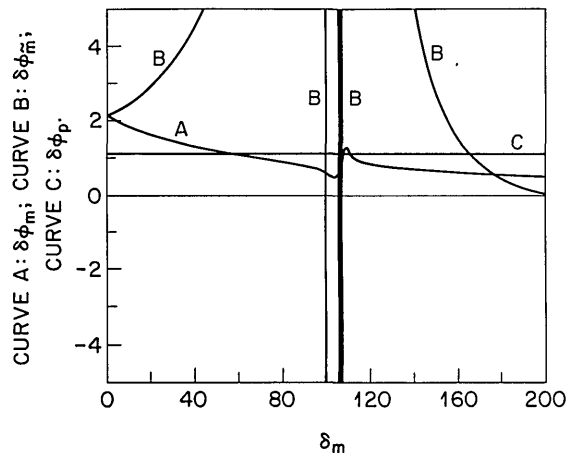


Fig. 18. Phase mismatch at nondegenerate frequencies for the case with $\Delta_p = 100$, $\beta = 40$, $F = 1$, $\Delta_{dhw} = 0$, $\delta k_m \neq 0$, and $L_a = 3000$. Curve A, $\delta\phi_m$; curve B, $\delta\phi_{\bar{m}}$; curve C, $\delta\phi_p$.

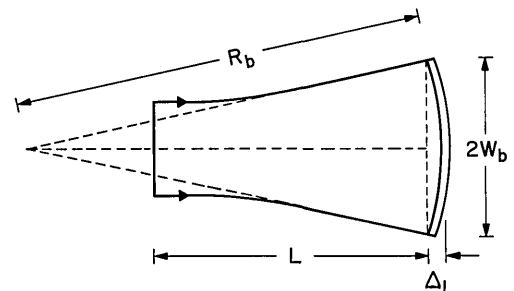


Fig. 19. Geometrical picture for self-focusing or defocusing. The radius of curvature of the beam phase front arising from defocusing is related to the beam waist and the advancement of the phase front Δ_L at the beam center.

the input beam waist and L is the medium length. The wave fronts are represented by the double solid curve. From the figure it is easily shown that for $R_b \gg \Delta_L$, $R_b = W_b^2/2\Delta_L$. The value of Δ_L can be related to $\delta\phi_p$ by means of $\Delta_L = \lambda(\delta\phi_p/2\pi)$. Hence, if the nonlinear phase shift is π , we have $\Delta_L = \lambda/2$. To minimize the intensity change within the medium, the medium length must be made short compared with R_b . We then conclude that a good design would require that $L < R_b = W_b^2/\lambda$. In practice this can be achieved by having a large input beam waist W_b . Of course, the trade-off is that one would have to increase the pump power in order to obtain the same pump intensity.

10. CONCLUSIONS

In summary, we have developed a quantum theory of non-degenerate multiwave mixing and applied it to predict the amount of squeezing generated in experiments that employ forward four-wave mixing in a Doppler-broadened two-level atomic vapor. In particular, we have focused on the single-beam case in which all the four interacting beams are spatially degenerate. This single-beam configuration is simple to implement in practice because one does not need to worry about proper alignment of the four beams. Furthermore, this simplicity makes it easier for a comparison to be made between the theory and the experiment.

Our theory is comprehensive in that it includes all the important physical effects such as loss, spontaneous emission, pump-probe phase mismatch, atomic collisions, Doppler broadening, Gaussian-beam intensity variation, and pump-intensity induced pump-probe focusing and defocusing. Of these, the effects of loss, spontaneous emission, and Gaussian-intensity variation were considered before by others interested in generating squeezed light through the interaction of an intracavity field with an atomic beam.^{11,12} The effect of pump-probe phase mismatch was considered by Levenson *et al.* in their squeezed-light generation experiment in an optical fiber.⁶ The effects of atomic collisions and Doppler broadening are somewhat unique to our atomic-vapor experiments and have not been considered before to our knowledge, except that the effect of collisions was included but not studied in detail by Reid and Walls.⁴ The effect of pump-intensity-induced pump-probe focusing and defocusing, though important in both atomic-beam and atomic-vapor experiments, has not been considered at all. Our theory and experiments indicate that this last effect can impose an important limitation on the maximum amount of achievable squeezing. This may explain why all earlier experiments that employed four-wave mixing interaction with atoms failed to agree with theories that do not take such an effect into account.^{7,11} This finding also has serious implications for squeezed-light generation using $\chi^{(3)}$ media whose nonlinear behavior is quite similar to that of the two-level atoms.

Our comprehensive theory has yielded a set of rules of thumb for achieving substantial squeezing in atomic media. These rules of thumb, described below, are not a set of precise equations but are bounds that predict a favorable region for the operation of experiments.

Rule A. It is usually good to work with the maximum available laser intensity. Let the normalized value of the

used laser intensity be β^2 . Then, for a given β^2 , in order to operate in the region where the medium is relatively lossless, one should choose the normalized pump detuning Δ_p such that $|\Delta_p| < \beta^2/2$ [see the paragraph after Eq. (6.14)]. This places an upper bound on $|\Delta_p|$.

Rule B. There is generally a maximum temperature that the cell containing the atomic vapor can be heated to. Suppose that this temperature gives a maximum value of $L_a = L_{\max}$. Then, in order to approach the long-medium regime in which the amount of squeezing is optimum, one should choose $|\Delta_p| < (L_{\max}/0.3)^{1/2}$ (see Subsections 7.A and 8.A). This gives another upper bound for $|\Delta_p|$ in addition to the one given by Rule A.

Rule C. If the Doppler half-width is Δ_{dhw} , then in order to avoid the effect of Doppler broadening one should choose $|\Delta_p| > 3\Delta_{\text{dhw}}$ (see Subsections 7.C and 8.F). This places a lower bound on $|\Delta_p|$.

Rule D. If one wants to see squeezing near the degenerate frequency such that the normalized probe detuning δ_m is less than 1, then one should have $|\Delta_p| > \beta^{4/3}/2$ in order to avoid spontaneous emission [see the paragraph before Eq. (6.14)]. The condition, however, can be relaxed to require $|\Delta_p| > 2\beta/\delta_m$ only if one is interested in squeezing at the nondegenerate frequency (see Subsection 8.D). This rule places a lower bound on both $|\Delta_p|$ and δ_m .

Rule E. In order to avoid the noisy region near the generalized Rabi frequency $\Delta_R = (\beta^2 F + \Delta_p^2)^{1/2}$, one should keep δ_m less than Δ_R (see Subsections 8.F and 8.G). This gives an upper bound for δ_m .

Rule F. The probe beam and the PCB see different refractive indices that are induced by the Gaussian-intensity pump beam. As a result probe modes become spatially mismatched as they propagate in the medium. In order to avoid this mode mismatching, one should keep $\delta_m < |\Delta_p|/2$, thus preventing the probe beams from having their frequencies too close to the atomic resonance (see Subsection 9.B). This rule gives another upper bound for δ_m , which is more stringent than that given by Rule E.

Rule G. In order to get a substantial amount of squeezing (>60%), if permitted by the above rules, one should have $|\Delta_p| > 100$ (see Subsection 8.B).

Rule H. In order to avoid the degrading effect of atomic collisions, one should keep the buffer-gas pressure low enough that the collision factor F is not less than ~ 0.5 (see Subsection 8.E).

Rule I. In order to avoid self-defocusing of the pump beam, which would reduce the pump intensity, it is good to keep the pump frequency blue detuned rather than red detuned (see Subsection 9.A). This rule can be relaxed if the pump intensity is high enough for substantial squeezing to occur on the blue side. This is because the amount of squeezing is not highly sensitive to the pump intensity when, at a particular vapor temperature, we are operating in a relatively lossless and noiseless regime where substantial squeezing occurs.

Rule J. The pump-beam intensity variation in the medium caused by diffraction should be kept to a minimum. This can be achieved by choosing the medium length to be smaller than the Rayleigh length. This rule is desirable in general and is not directly related to the self-focusing or defocusing problem.

Rule K. Pump self-focusing or defocusing can change the pump intensity in the medium, thus limiting the amount of squeezing generated. If the LO is derived

from the input pump beam, then the mode mismatch between the LO and the maximally squeezed probe mode can also limit the amount of observed squeezing when there is self-focusing or defocusing. The latter problem can, however, be resolved by using the transmitted pump as the LO, as discussed in Subsection 9A. Moreover, it turns out that, when the former problem is avoided, so is the latter. In order to solve the former problem, one should design the vapor cell in such a way that the vapor length L obeys $L < W_b^2/\lambda$, where W_b is the effective beam radius (see Subsection 9C). With this design the maximum amount of achievable squeezing will be ultimately limited only by the pump-probe mode mismatch in the medium, which is caused by pump-intensity-induced pump and probe focusing or defocusing. The effect of pump-probe mode mismatch cannot be circumvented as long as a Gaussian-intensity pump beam is employed.

This completes the set of rules of thumb. In general, the better one can simultaneously satisfy these rules, the better will the observed squeezing be. What is then the ultimate limit on achievable squeezing? Our simple treatment of pump-intensity-induced pump and probe focusing or defocusing seems to indicate that one may be able to obtain only up to 75% squeezing in atomic-vapor experiments that employ a Gaussian-beam pump.

APPENDIX A

In this appendix we describe the method used for including the effect of Doppler broadening in our calculations. The effect can be taken into account by first replacing the frequency-independent atomic-number density ρ_a in Eq. (2.17) with a frequency-dependent atomic-number density per unit normalized frequency $\rho_a(\Delta_d)$, as given by

$$\rho_a(\Delta_d) = \rho_a \frac{1}{\sqrt{\pi}(ku/\gamma_\perp)} \exp\left[-\left(\frac{\Delta_d}{ku/\gamma_\perp}\right)^2\right], \quad (\text{A1})$$

where ρ_a is the total atomic-number density, $k = \Omega_p/c$, and u is the root-mean-square Doppler velocity given in terms of the Boltzmann constant k_B , the absolute temperature T , and the mass of the atom M by $u = (2k_B T/M)^{1/2}$. In Eq. (A1), $\Delta_d = (\omega_{av} - \omega_{as})/\gamma_\perp$, where ω_{av} is the Doppler-shifted resonance frequency for the group of atoms that we are interested in and ω_{as} is the resonance frequency for a stationary atom. We then replace the atomic frequency ω_a in Δ_p by $\gamma_\perp \Delta_d + \omega_{as}$ so that Δ_p now becomes $\Delta_{ps} - \Delta_d$, where $\Delta_{ps} = (\Omega_p - \omega_{as})/\gamma_\perp$. The integration $\int_{-\infty}^{\infty} d\Delta_d$ is then performed over the expressions for $\check{\gamma}_m$, \check{X}_m , $\check{\gamma}_{\bar{m}}$, $\check{X}_{\bar{m}}$, Λ_m , $\Lambda_{\bar{m}}$, R_m , and $R_{\bar{m}}$, yielding a new set of mode-coupling coefficients and noise correlations. The effect of Doppler broadening is properly included when this new set is used to calculate $\alpha_m(L)$ by Eq. (3.11). This procedure is equivalent to performing the sum over atoms in Ref. 2, with each atom taken to have a different Doppler-shifted resonance frequency.

We shall use the $\exp(-1)$ half-width of the Doppler-velocity distribution as a convenient parameter in our calculations. This normalized half-width is given by ku/γ_\perp and will be denoted as Δ_{dhw} . It is related to the normalized FWHM (Δ_{FWHM}) of the Doppler-velocity distribution by $\Delta_{\text{dhw}} = \Delta_{\text{FWHM}}/2\sqrt{\ln 2}$.

APPENDIX B

In this appendix we describe the method for taking into account the Gaussian-intensity variation of the pump beam. We denote the intensity variation of the pump beam by $I_p(r) = I_{pk} \exp(-2r^2/W_b^2)$, where r is the radial displacement and W_b is a parameter specifying the effective beam radius. $I_p(r)$ can also be expressed in terms of the pump power P_0 through $I_p(r) = P_0 U^2(r)$, where

$$U^2(r) = \frac{1}{W_b^2 \pi/2} \exp\left[-2\left(\frac{r}{W_b}\right)^2\right]. \quad (\text{B1})$$

The relationship between I_{pk} and P_0 is then given by $I_{pk} = 2P_0/W_b^2 \pi$. Let the electric field operator, expressed in terms of the $\pm z$ -propagating plane-wave modes, be given by

$$\hat{E}_p(x, y, z, t) = \sum_m C_m \hat{a}_m(t) \exp(ik_m z) + \text{H.c.}, \quad (\text{B2})$$

where C_m is a mode-dependent constant and H.c. denotes a Hermitian conjugate. The electric field operator expressed in terms of the $\pm z$ -propagating Gaussian-intensity modes will then have the form

$$\hat{E}_g(r, z, t) = \sum_m C_m \hat{a}_m(t) Q(r) \exp(ik_m z) + \text{H.c.}, \quad (\text{B3})$$

where the mode function $Q(r)$ is proportional to $U(r)$. The proportionality constant can be obtained by requiring that

$$\begin{aligned} \int dr dz [2\pi r \hat{E}_g(r, z, t)]^2 &= \int dx dy dz [\hat{E}_p(x, y, z, t)]^2 \\ &= |C_m|^2 [\hat{a}_m^\dagger \hat{a}_m + \hat{a}_m \hat{a}_m^\dagger] A_Q L_Q, \end{aligned} \quad (\text{B4})$$

where $A_Q = \int dx dy$, $L_Q = \int dz$, and $A_Q L_Q$ is the volume of quantization. Here A_Q is assumed to be infinitely large. The constraint Eq. (B4) yields $Q(r) = A_Q U(r)$. Hence the treatment for including the effect of Gaussian-intensity variation first calls for the replacement of I_p in Eq. (2.14) by $I_p(r)$ so that β^2 becomes $\beta_{pk}^2 U^2(r)$ with $\beta_{pk}^2 = 2I_{pk}/I_{sa}$ and then having g_a in Eq. (2.18) replaced by $g_a U(r)$ so that α_a becomes $\alpha_a U(r)$, with α_a now denoting $\rho_a |\mu_d|^2 \omega_a / 2\hbar \epsilon_0 c \gamma_\perp$, ρ_a being the total atomic density. After all these replacements the procedure ends with the integration $\int_0^\infty dr 2\pi r$ performed on $\check{\gamma}_m$, \check{X}_m , $\check{\gamma}_{\bar{m}}$, $\check{X}_{\bar{m}}$, Λ_m , $\Lambda_{\bar{m}}$, R_m , and $R_{\bar{m}}$, resulting in a new set of mode-coupling coefficients and noise correlations for calculating $\alpha_m(L)$. We note that the use of the same mode function $U(r)$ for both $I_p(r)$ and $\{\check{g}_m^A, \check{g}_{\bar{m}}^A\}$ implies that the probe-beam modes are the same as the pump-beam mode.

The above treatment is valid provided that we assume that δk_m^s in Eqs. (2.6) and (2.7) is independent of the transverse coordinates. However, in reality the value of δk_m^s depends on the transverse position within the beam. Thus one really needs to integrate $\check{X}_m \exp(-i\delta k_m^s Z)$ transversely in order to obtain an effective coefficient. The resulting coefficient will be z dependent, and the method of solution presented in Section 3 can no longer be used. A proper treatment requires one to integrate the equation of motion for $\alpha_m(Z)$ numerically. In this paper we simply let δk_m^s be given by Eq. (2.34) but with the integrated values of $\check{\gamma}_{lm}$, $\check{\gamma}_{l\bar{m}}$, and $\check{\gamma}_{lp}$.

ACKNOWLEDGMENTS

This work was supported in part by the National Science Foundation under grants ECS-8718970 and EET-8715275; that of S.-T. Ho was also supported by the Newport Research Award.

J. H. Shapiro is also with the Research Laboratory of Electronics, Massachusetts Institute of Technology, Cambridge, Massachusetts 02139.

REFERENCES

1. S.-T. Ho, P. Kumar, and J. H. Shapiro, *Phys. Rev. A* **37**, 2017 (1988).
2. S.-T. Ho, P. Kumar, and J. H. Shapiro, "Quantum theory of nondegenerate multiwave mixing II: derivation and quantization of slowly varying spatiotemporal coupled-mode equations," submitted to *Physical Review A*.
3. S.-T. Ho, N. C. Wong, J. H. Shapiro, and P. Kumar, in *Digest of Optical Society of America Annual Meeting* (Optical Society of America, Washington, D.C., 1988), paper TuL1, p. 84; S.-T. Ho, N. C. Wong, and J. H. Shapiro, in *Coherence and Quantum Optics VI*, J. H. Eberly, L. Mandel, and E. Wolf, eds. (Plenum, New York, 1989); M. W. Maeda, P. Kumar, and J. H. Shapiro, *J. Opt. Soc. Am. B* **4**, 1501 (1987); *Opt. Lett.* **12**, 161 (1987); *Phys. Rev. A* **32**, 3803 (1985).
4. M. D. Reid and D. F. Walls, *Phys. Rev. A* **31**, 1622 (1985); **34**, 4929 (1986).
5. R. W. Boyd, M. G. Raymer, P. Narum, and D. J. Harter, *Phys. Rev. A* **24**, 411 (1981).
6. G. J. Milburn, M. D. Levenson, R. M. Shelby, S. H. Perlmutter, R. G. DeVoe, and D. F. Walls, *J. Opt. Soc. Am. B* **4**, 1476 (1987).
7. R. S. Bondurant, P. Kumar, J. H. Shapiro, and M. Maeda, *Phys. Rev. A* **30**, 343 (1984); M. W. Maeda, P. Kumar, and J. H. Shapiro, *J. Opt. Soc. Am. B* **4**, 1501 (1987).
8. P. Kumar and J. H. Shapiro, *Phys. Rev. A* **30**, 1568 (1984).
9. S.-T. Ho, P. Kumar, and J. H. Shapiro, *Phys. Rev. A* **35**, 3982 (1987).
10. D. F. Walls and P. Zoller, *Phys. Rev. Lett.* **47**, 709 (1981); R. Loudon, *Opt. Commun.* **49**, 24 (1984); M. J. Collett, D. F. Walls, and P. Zoller, *Opt. Commun.* **52**, 145 (1984); A. Heidmann and S. Reynaud, *J. Phys. (Paris)* **46**, 1937 (1985).
11. R. E. Slusher, B. Yurke, P. Grangier, A. LaPorta, D. F. Walls, and M. Reid, *J. Opt. Soc. Am. B* **4**, 1453 (1987).
12. M. Xiao, H. J. Kimble, and H. J. Carmichael, *J. Opt. Soc. Am. B* **4**, 1546 (1987).